Recent advances in cancer imaging

Brian P. Hobbs
bphobbs@mdanderson.org

Department of Biostatistics, MD Anderson Cancer Center

February 3, 2016

THE UNIVERSITY OF TEXAS
MD Anderson Cancer Center
Making Cancer History®

Integrative Analysis of NeuroImaging and Genetics

UTHealth The University of Texas Health Science Center at Houston

Integrative Bayesian Analysis of Neuroimaging-Genetic Data

Shabnam Azadeh, Brian P. Hobbs, Frederick G. Moeller, David Nielsen , Veerabhadran Baladandayuthapani.

THE UNIVERSITY OF TEXAS MD Anderson Cancer Center

Significance: Explore underlying neurobiological information of white matter integrity of the brain.

Statistical goals: Develop a novel integrated framework to combine imaging and genetic data in cocaine dependence.

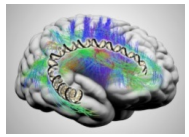

Data: Genetic: 21 candidate genetic variants in 17 genes, clinical and demographic (sex, age, group).
Imaging: Diffusion Tensor Imaging (DTI) of entire Brain **(more than 7 millions voxels)**.

iBANG method:

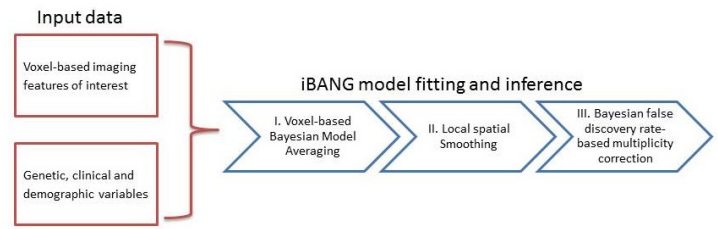

iBANG method:

$$\boldsymbol{Y}(\nu) = \alpha + \boldsymbol{X}_j \boldsymbol{\beta}_j(\nu) + \sigma\boldsymbol{\epsilon}$$

1. Parameters priors:

$$p(\alpha, \sigma) \propto \sigma^{-1}$$

$$p(\boldsymbol{\beta}_j|\alpha, \sigma, M_j) \sim N_{k_j}(\mathbf{0}, \sigma^2(g\mathbf{X_j}'\mathbf{X_j})^{-1}),$$

$$g = 1/max\left\{n, k^2\right\}$$

2. Model space prior:

A uniform prior distribution

2^k possible models

$$P(M_j) = p_j = 2^{-k}.$$

Significate Regions

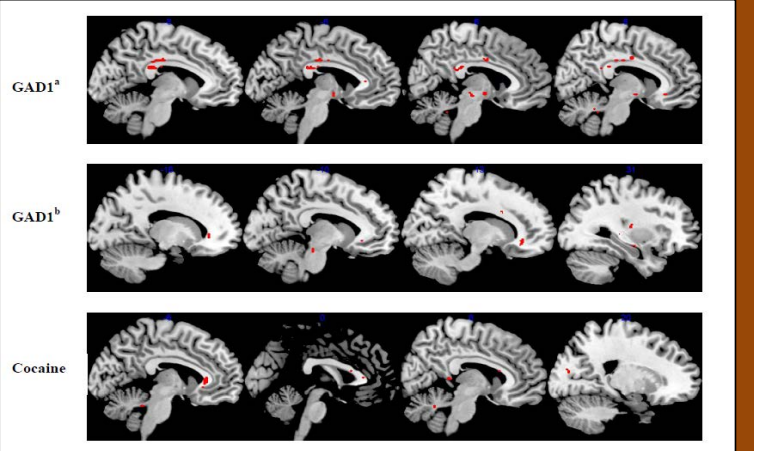

Magnitude and Direction of FA Changes in Corpus Callosum

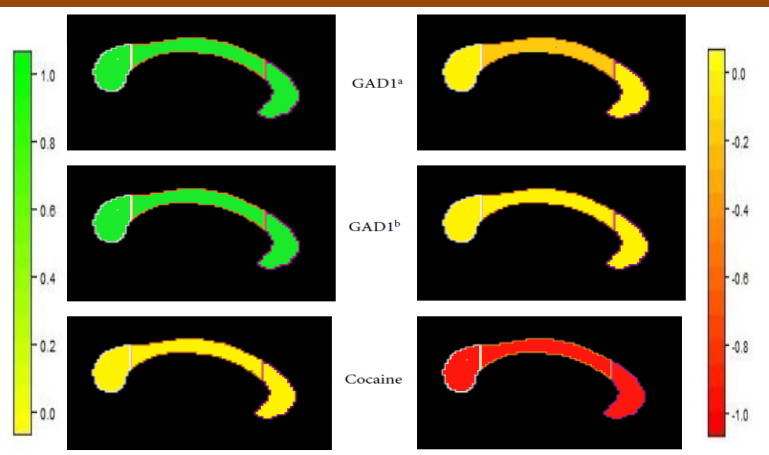

Integrative Analysis of NeuroImaging and Genetics

UTHealth The University of Texas Health Science Center at Houston

Integrative Bayesian Analysis of Neuroimaging-Genetic Data

Shabnam Azadeh, Brian P. Hobbs, Frederick G. Moeller, David Nielsen , Veerabhadran Baladandayuthapani.

THE UNIVERSITY OF TEXAS MD Anderson Cancer Center

Significance: Explore underlying neurobiological information of white matter integrity of the brain.

Statistical goals: Develop a novel integrated framework to combine imaging and genetic data in cocaine dependence.

Data: Genetic: 21 candidate genetic variants in 17 genes, clinical and demographic (sex, age, group).
Imaging: Diffusion Tensor Imaging (DTI) of entire Brain **(more than 7 millions voxels)**.

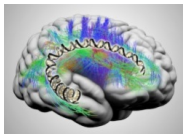

Sparse Functional Modeling of "Washout" for Detection of Adrenal Cancer

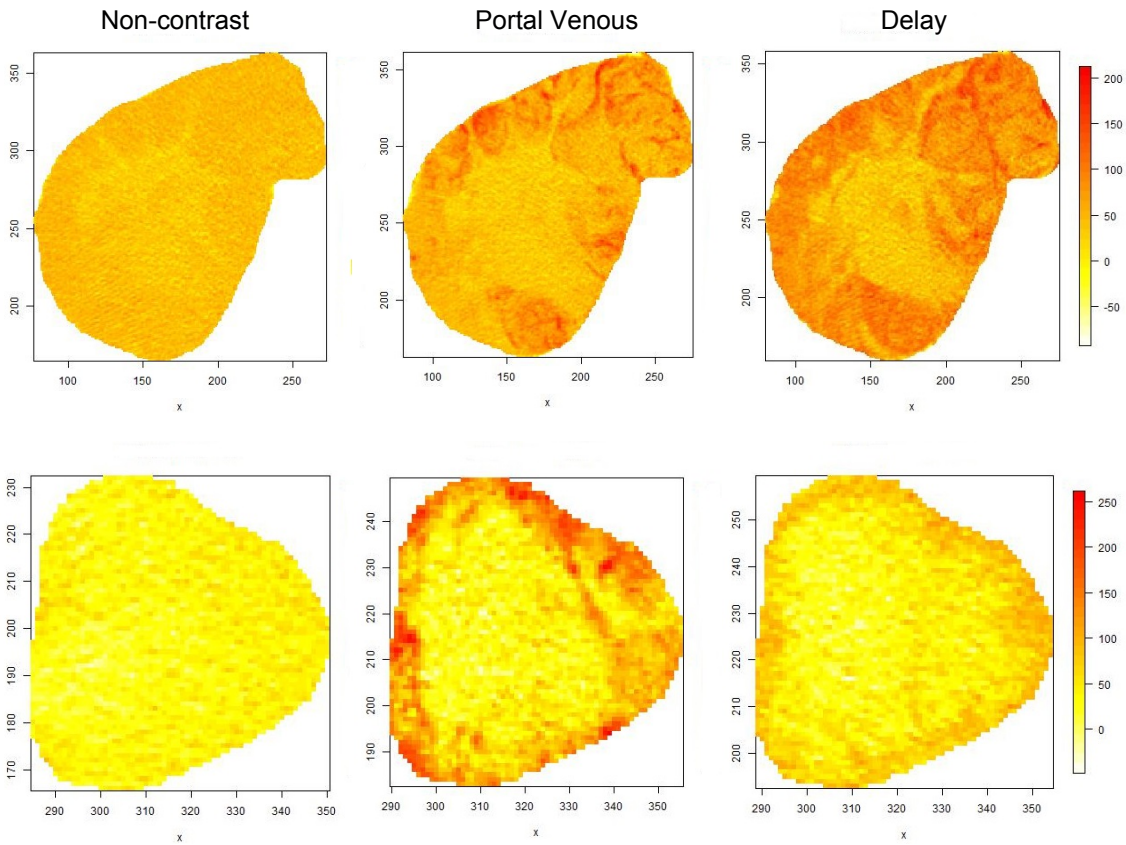

Distributions of HU density over three successive scans within two ROIs: one containing a malignant (top) the other a benign (bottom) adrenal lesion. In contrast to the benign lesion, the malignant tissues exhibit relatively high HU density in the noncontrast scan as well as the relative absence of "washout" between portal venous and delay scans.

Identify RT Dosimetries associated with ORN

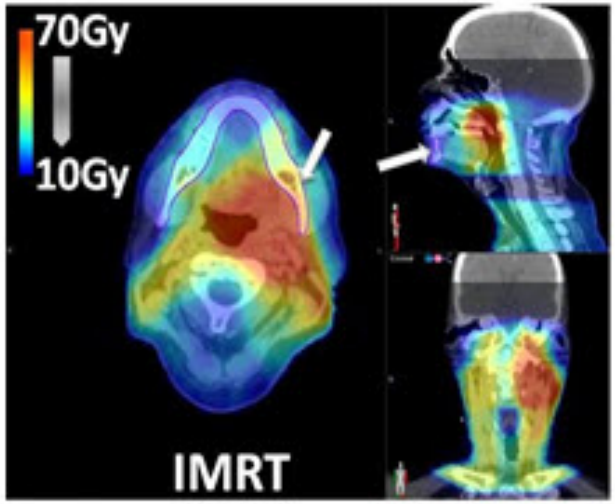

Radiation dose map for IMRT. The mandible (white arrows) receives substantial EBRT dose. IMRT provides for a relatively large low dose area of exposure with focal areas, which exceed 40Gy.

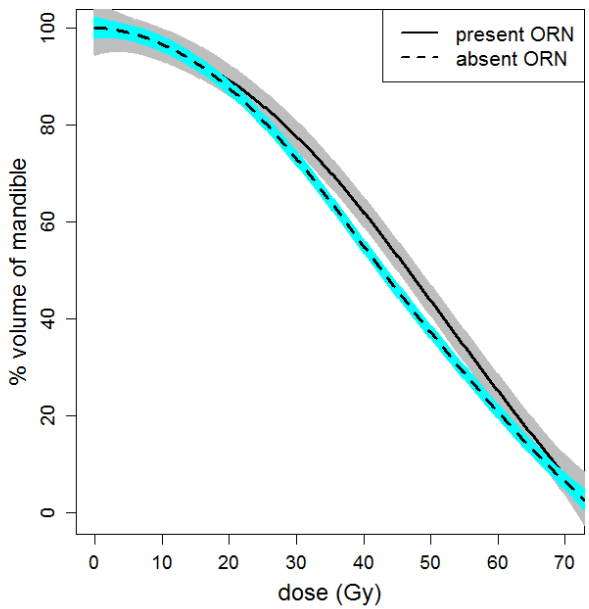

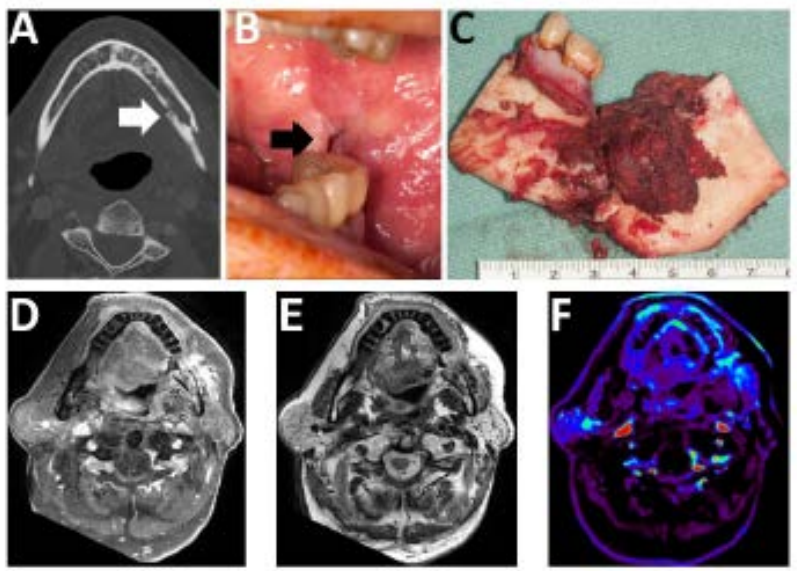

DCE-MRI Mandible Vascularity During External Beam RT

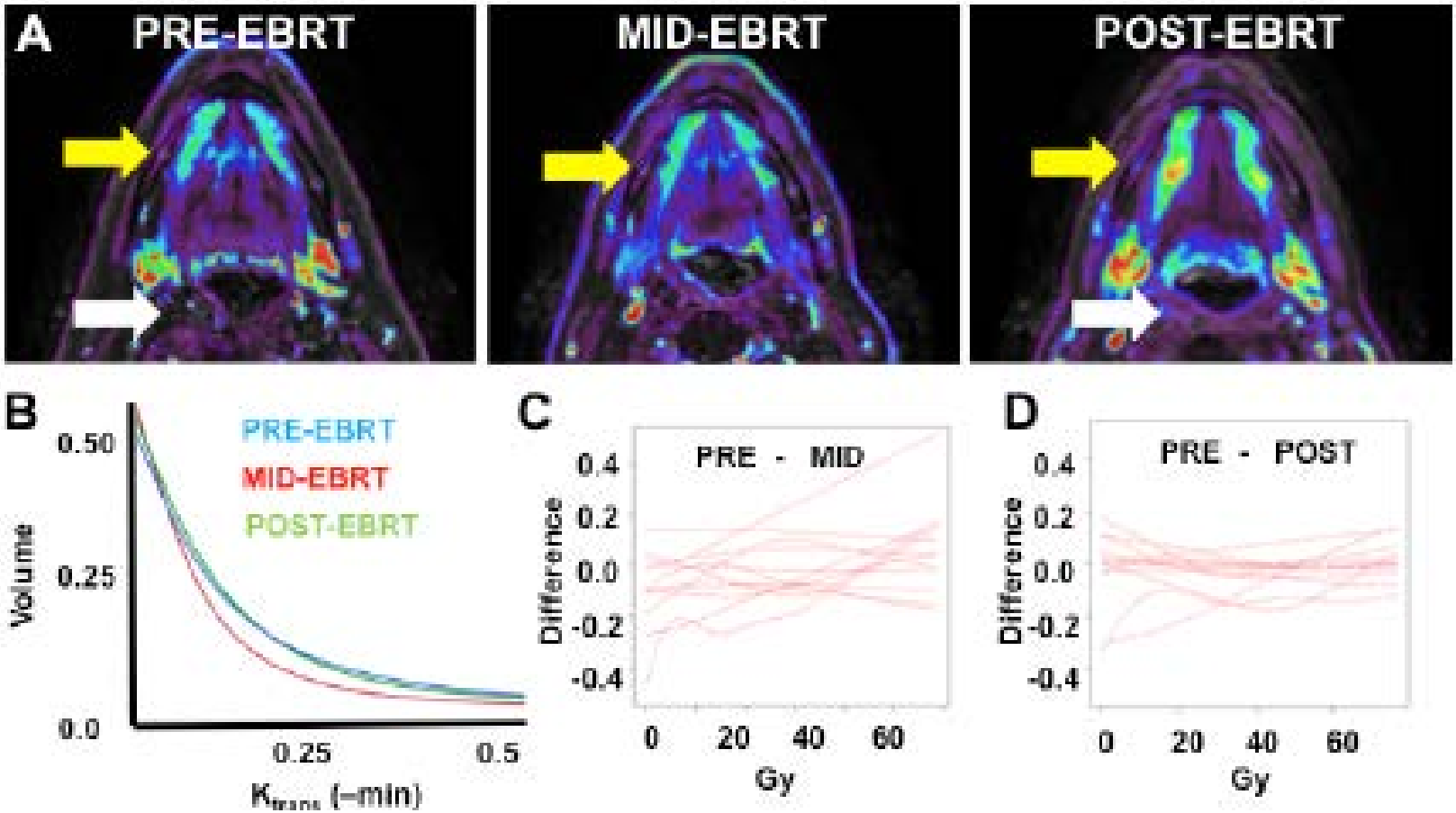

Sandulache VC, Hobbs BP, et al. Dynamic contrast enhanced magnetic resonance imaging (DCE-MRI) detects acute radiotherapy-induced alterations in mandibular bone microvasculature, *Nature Scientific Reports*

Pulmonary Radiation Response on FDG PET/CT

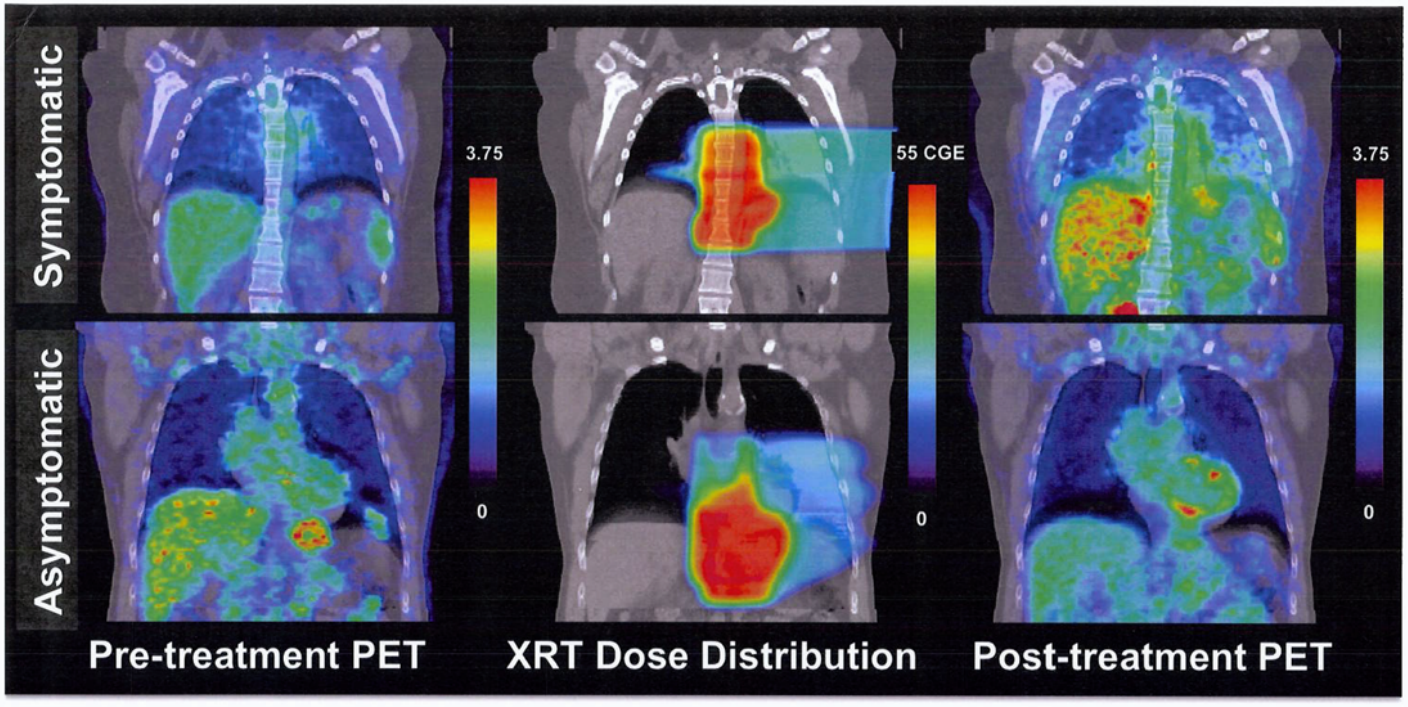

Hypothesis: Pre-treatment pulmonary inflammation, assessed from FDG PET imaging, predicts for post-treatment symptomatic radiation pneumonitis.

ASTRO ANNUAL MEETING SCIENCE BASED. PATIENT DRIVEN
Advancing Patient Care *through* iNNOVATiON

High-throughput extraction of quantitative image features

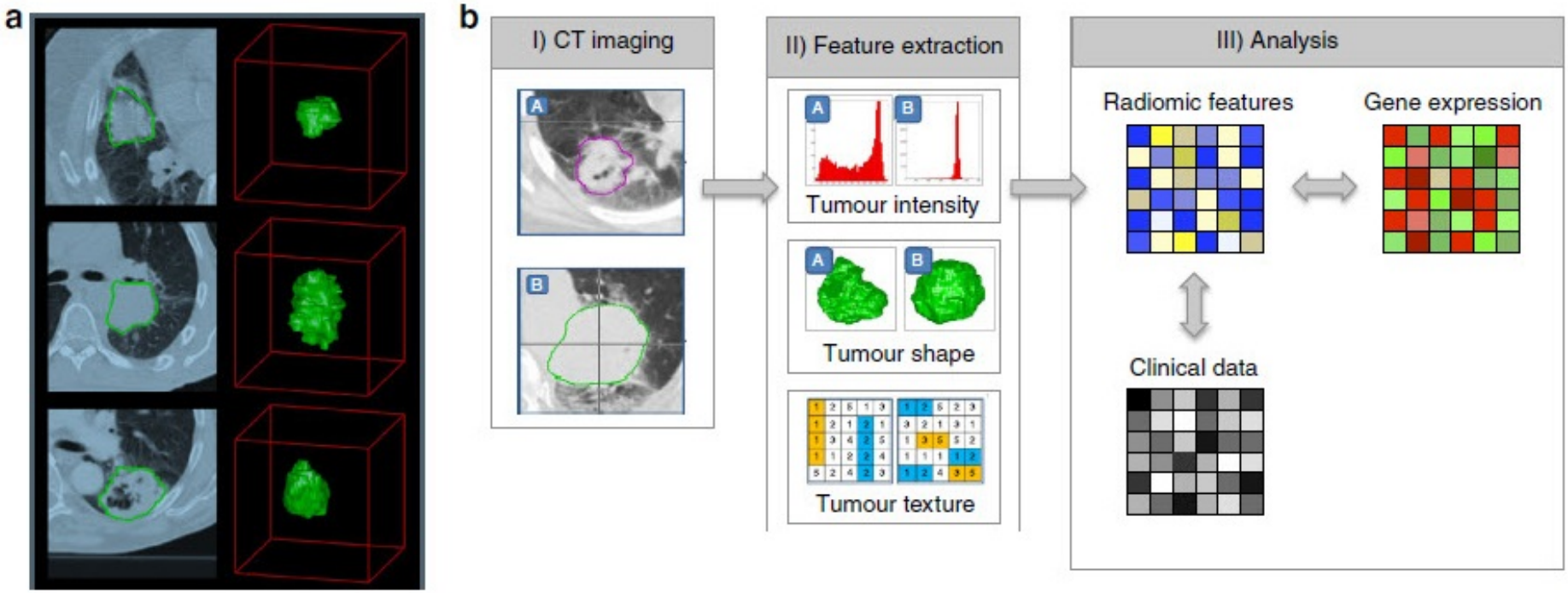

Figure 1 | Extracting radiomics data from images. (**a**) Tumours are different. Example computed tomography (CT) images of lung cancer patien images with tumour contours left, three-dimensional visualizations right. Please note strong phenotypic differences that can be captured with rou imaging, such as intratumour heterogeneity and tumour shape. (**b**) Strategy for extracting radiomics data from images. (I) Experienced physician contour the tumour areas on all CT slices. (II) Features are extracted from within the defined tumour contours on the CT images, quantifying tu intensity, shape, texture and wavelet texture. (III) For the analysis the radiomics features are compared with clinical data and gene-expression da

Aerts et al., Nature Communications, 2014; Parmar et al. PLOS ONE, 2014

Immune Pathology Markers

254 patients with no neoadjuvant chemotherapy and known immune pathology features

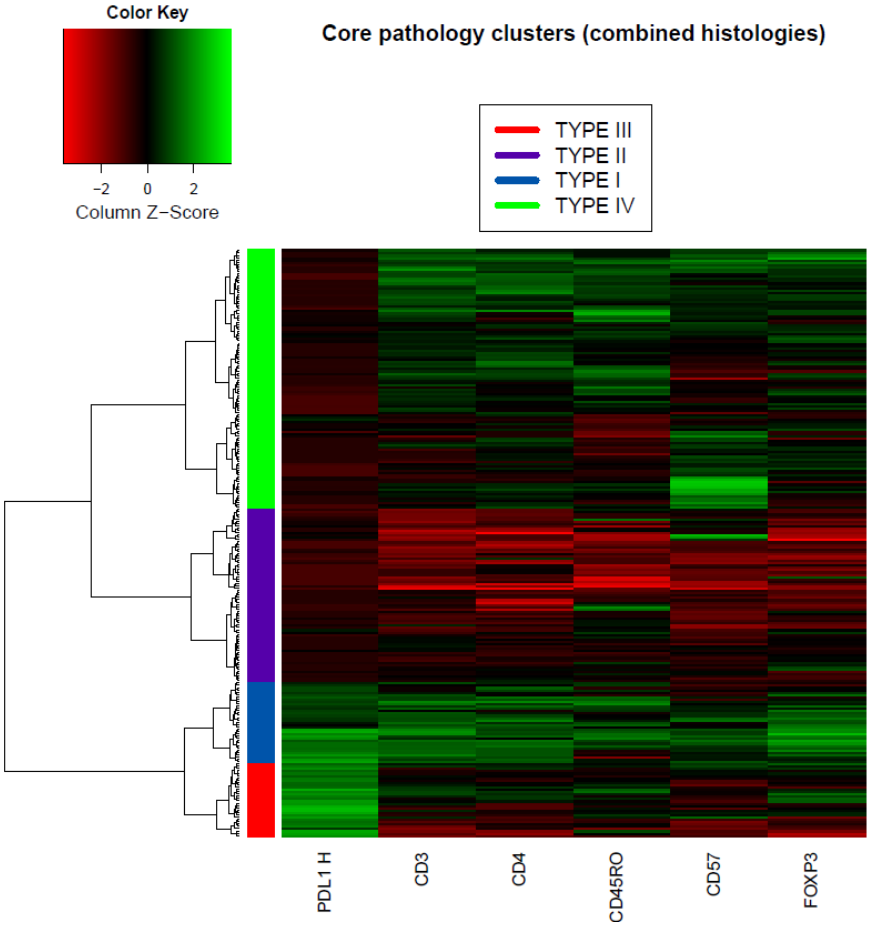

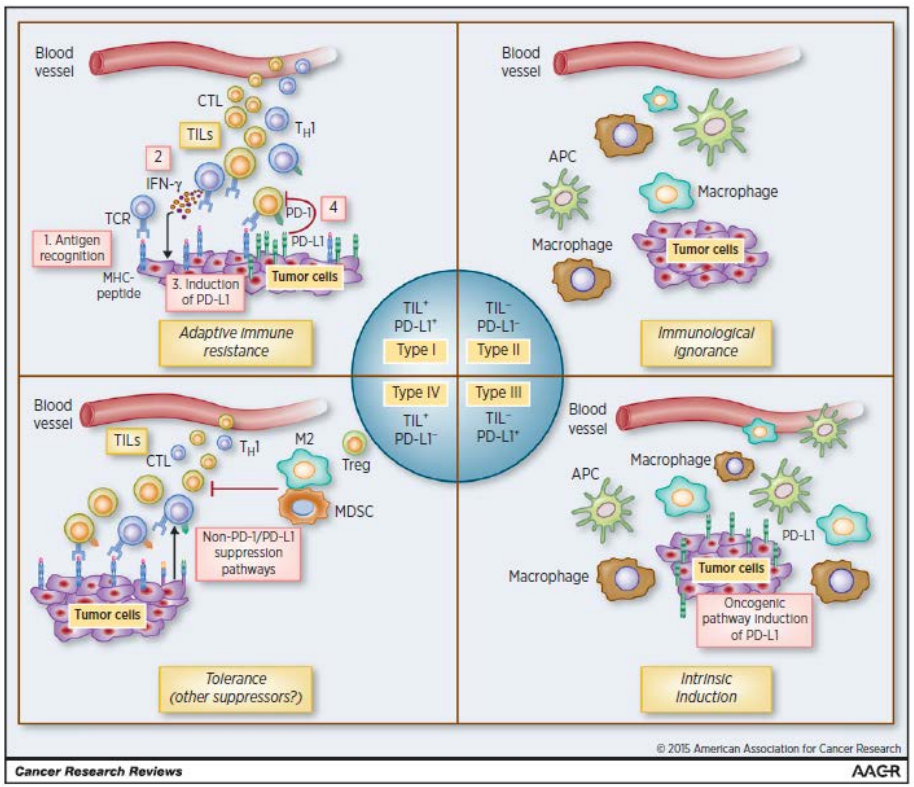

Radiomics Clustering

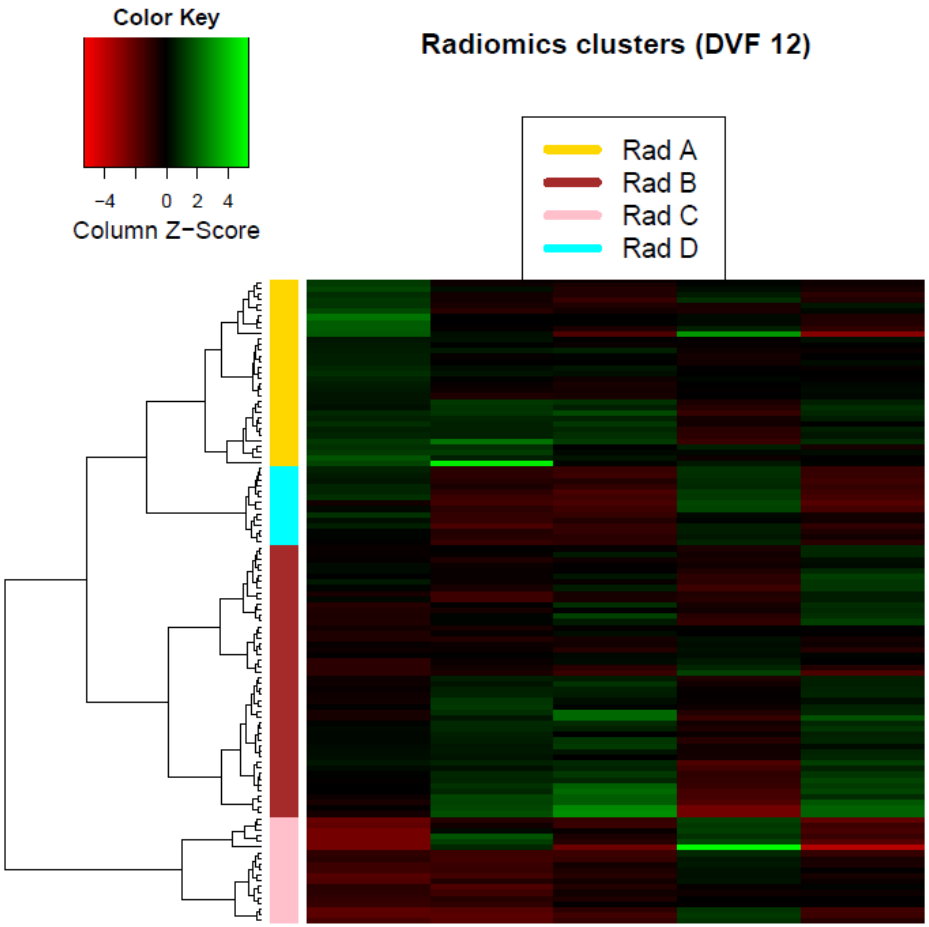

Pathology Clustering

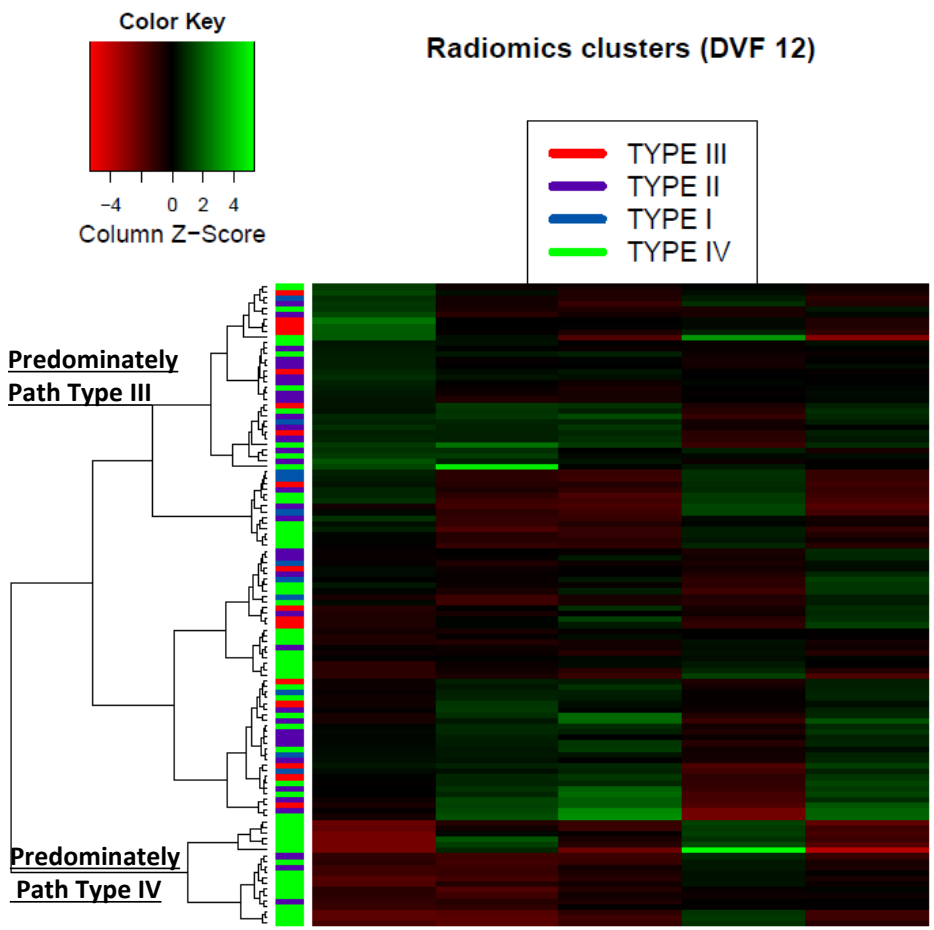

Training Dataset

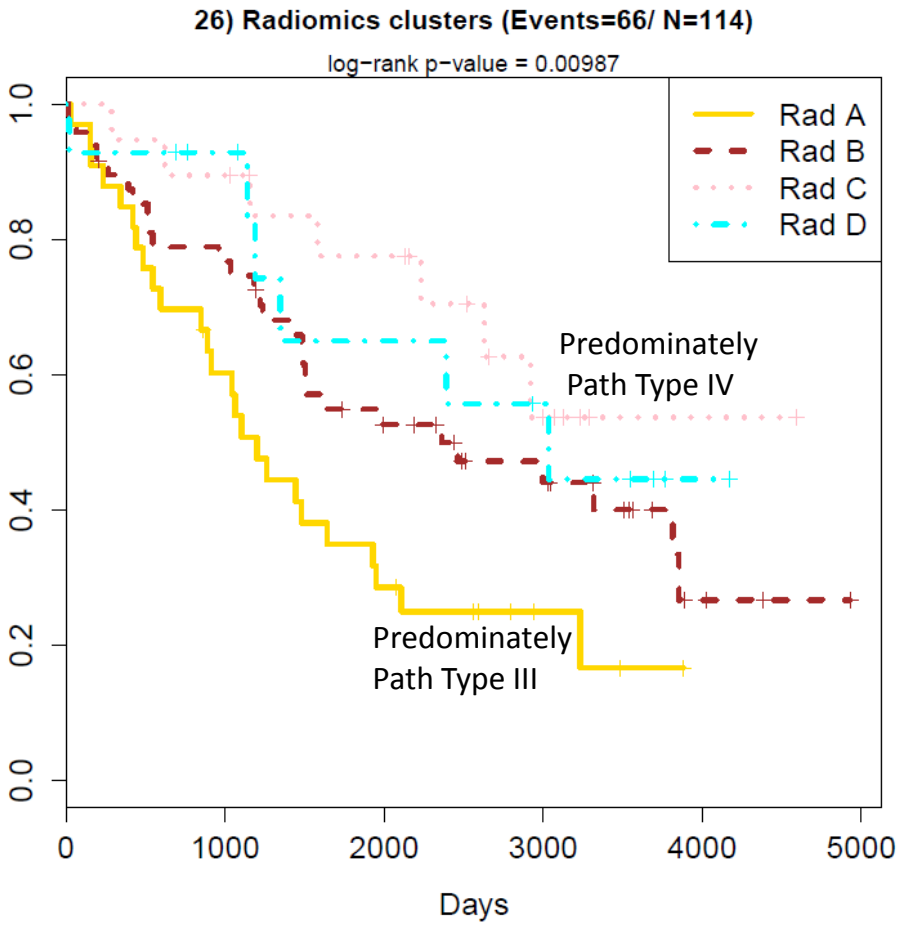

Validation Dataset

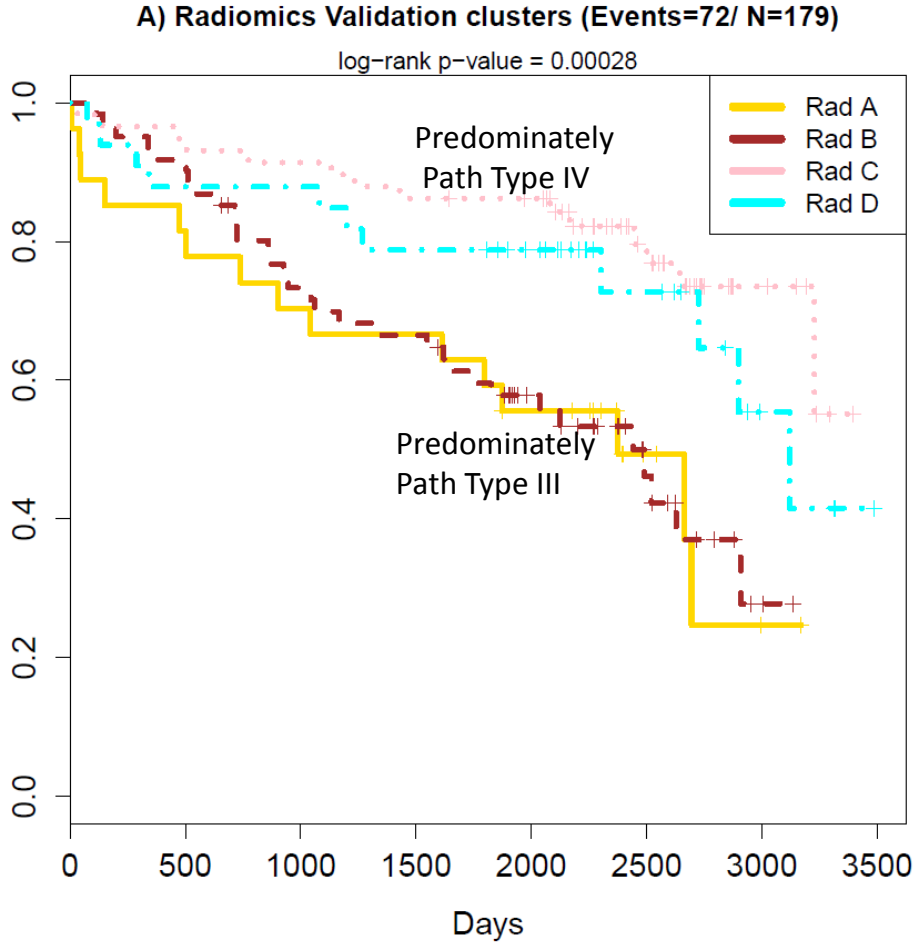

Outline: Liver Perfusion Imaging

1. Acquisition of perfusion characteristics in liver using CT

2. Classification of spatially correlated targets (identification metastatic sites)
   a. ROI level inference
   b. Voxel-wise Posterior Probability Maps

3. Functional Spatiotemporal modeling to integrate multiple scans

Chaan Ng, MD

Yuan Wang, PhD

Jianhua Hu, PhD

Nan Chen, PhD

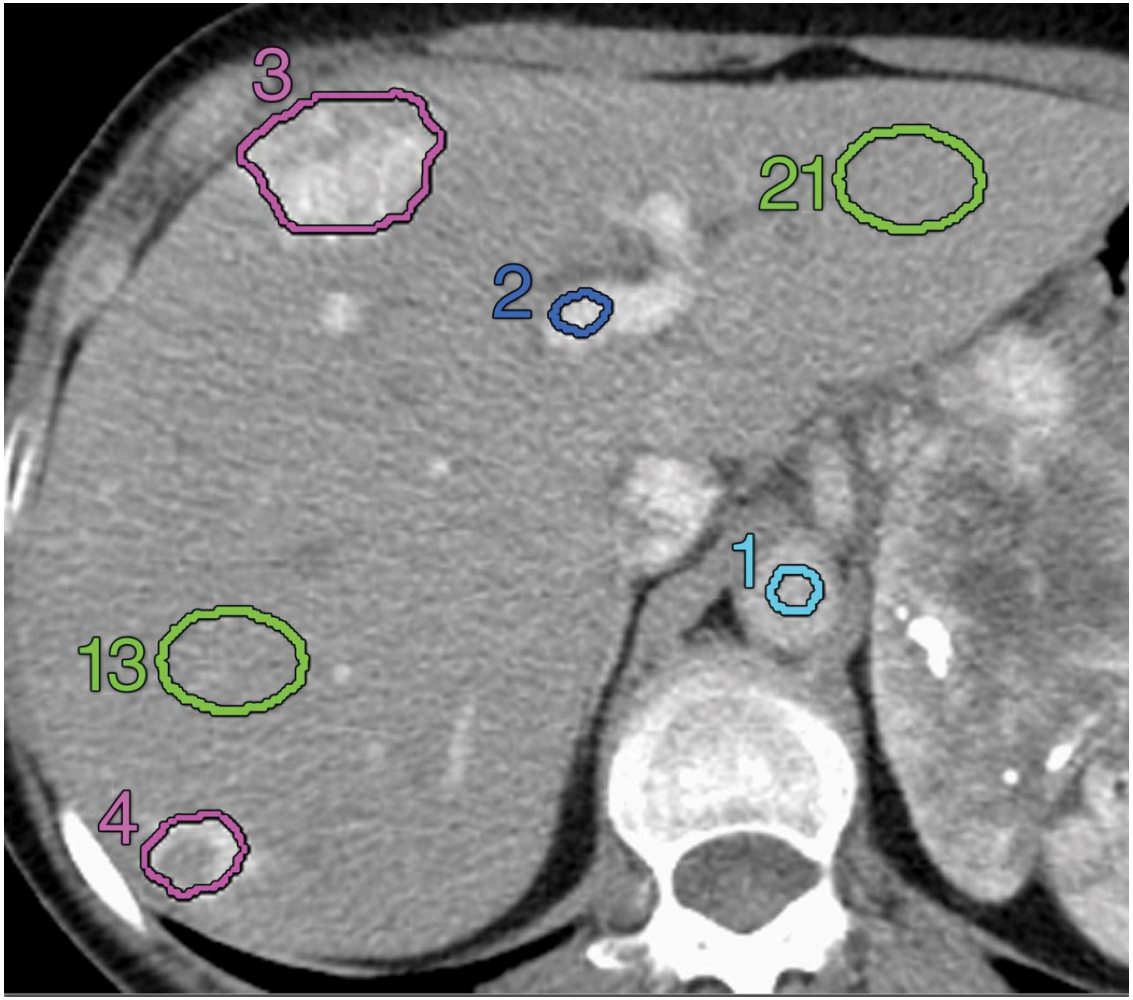
3
21
2
1
13
4

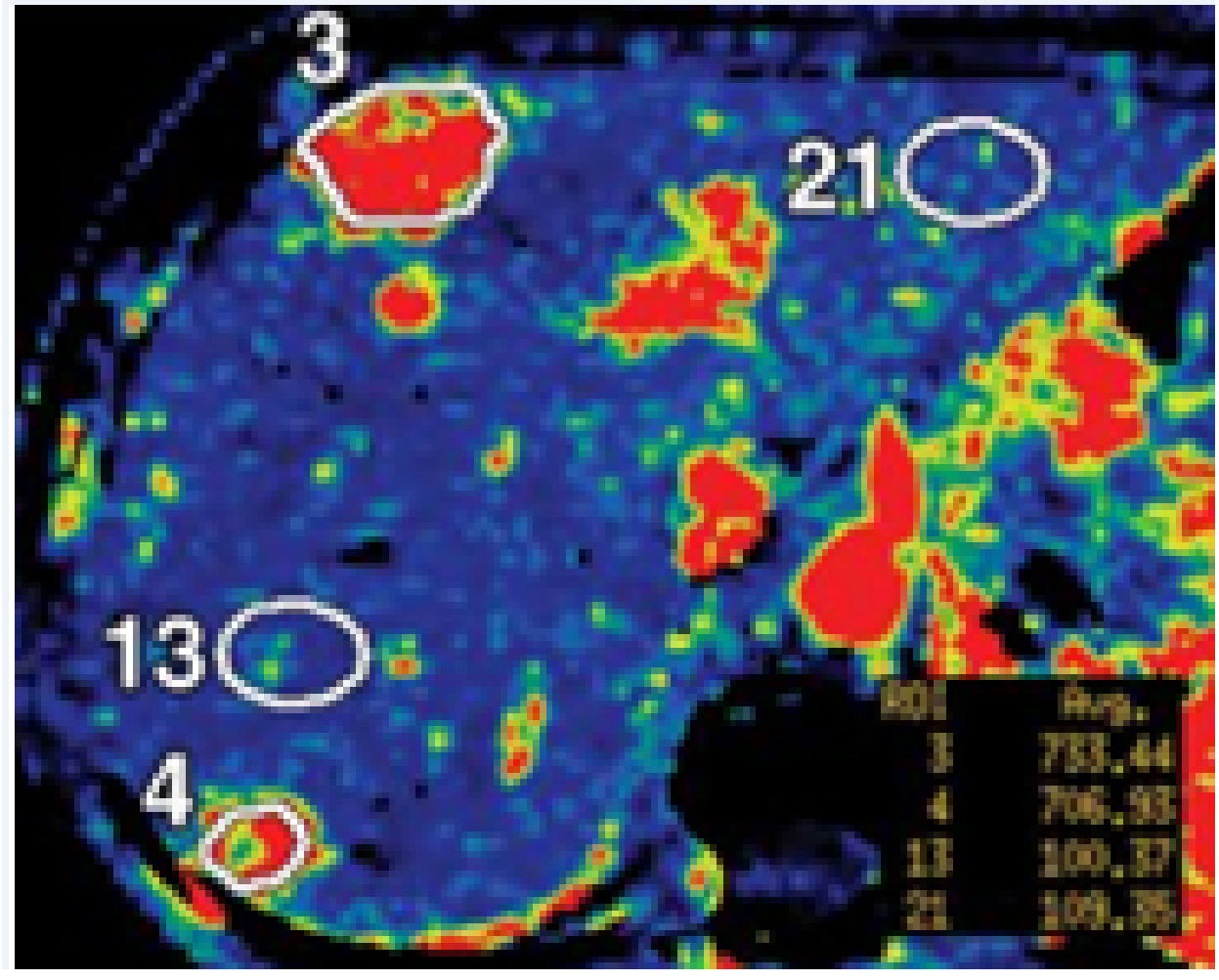
3
21
13
4
Avg.
753.44
706.93
100.37
109.35

CT perfusion acquisition

CTp image

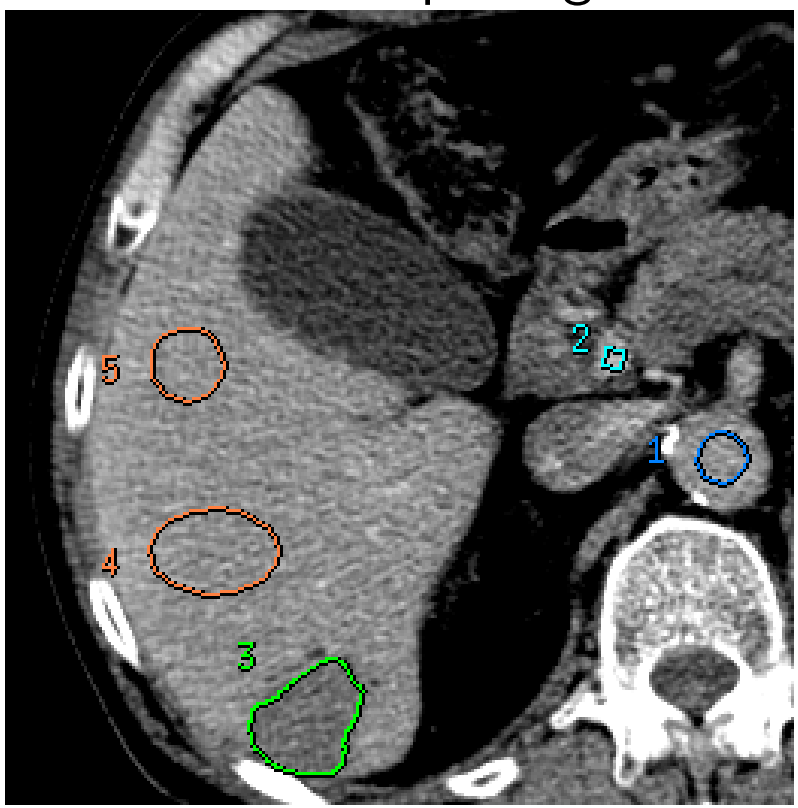

Time-attenuation curves

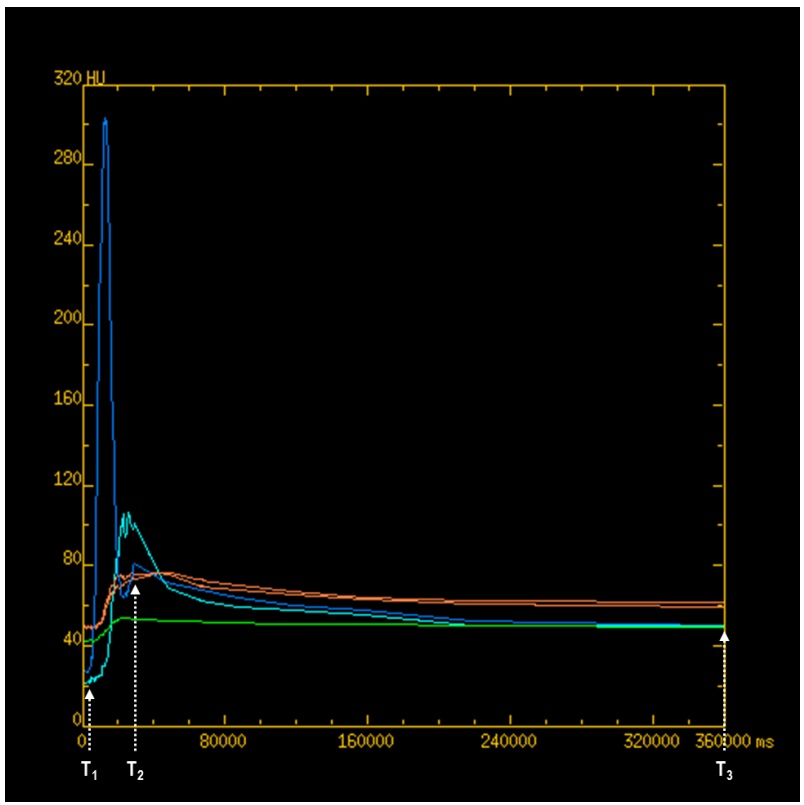

Hepatic perfusion characteristics

Physiological modeling with contrast agent as physiological indicator:

- blood flow (BF) *rate in mL/min per 100g microcirculation*
- blood volume (BV) *in mL/100g concentration*
- mean transit time (MTT) *duration in seconds*
- permeability (PS) *mL/min per 100 g capillary permeability and leakage (extracellular) space*
- hepatic arterial fraction (HAF) *extent of blood supply from aorta*

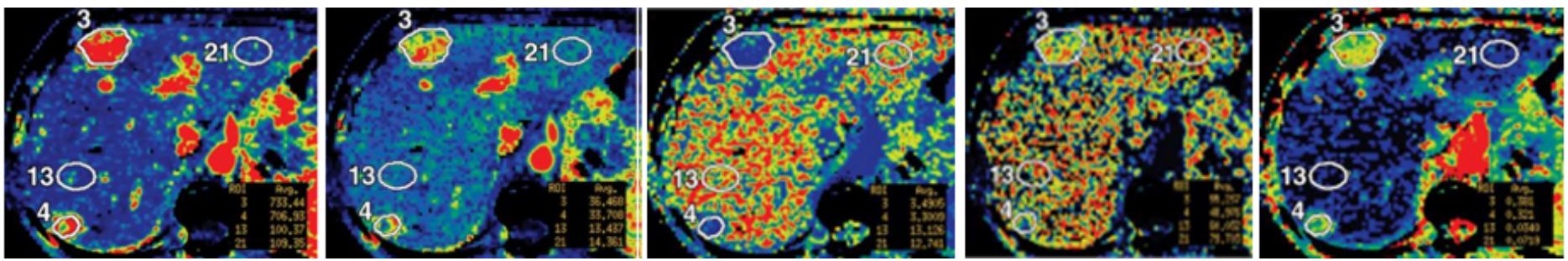

Miles, KA et al. (2000). Application of CT in the investigation of angiogenesis

Miles, KA (2002). Functional CT in oncology.

Perfusion Imaging

Tissue perfusion plays a critical role in oncology

- Cancerous cell growth and migration requires the proliferation of networks of new blood vessels through the process of angiogenesis
- triggers modifications to the vasculature of surrounding host tissue

Hepatic perfusion characteristics

- provide physiological correlates for neovascularization induced by tumor angiogenesis
- quantitative basis for characterizing vasculature changes in the tumor microenvironment
- implications for cancer diagnosis, treatment monitoring, and disease prognostication and pathophysiological understanding

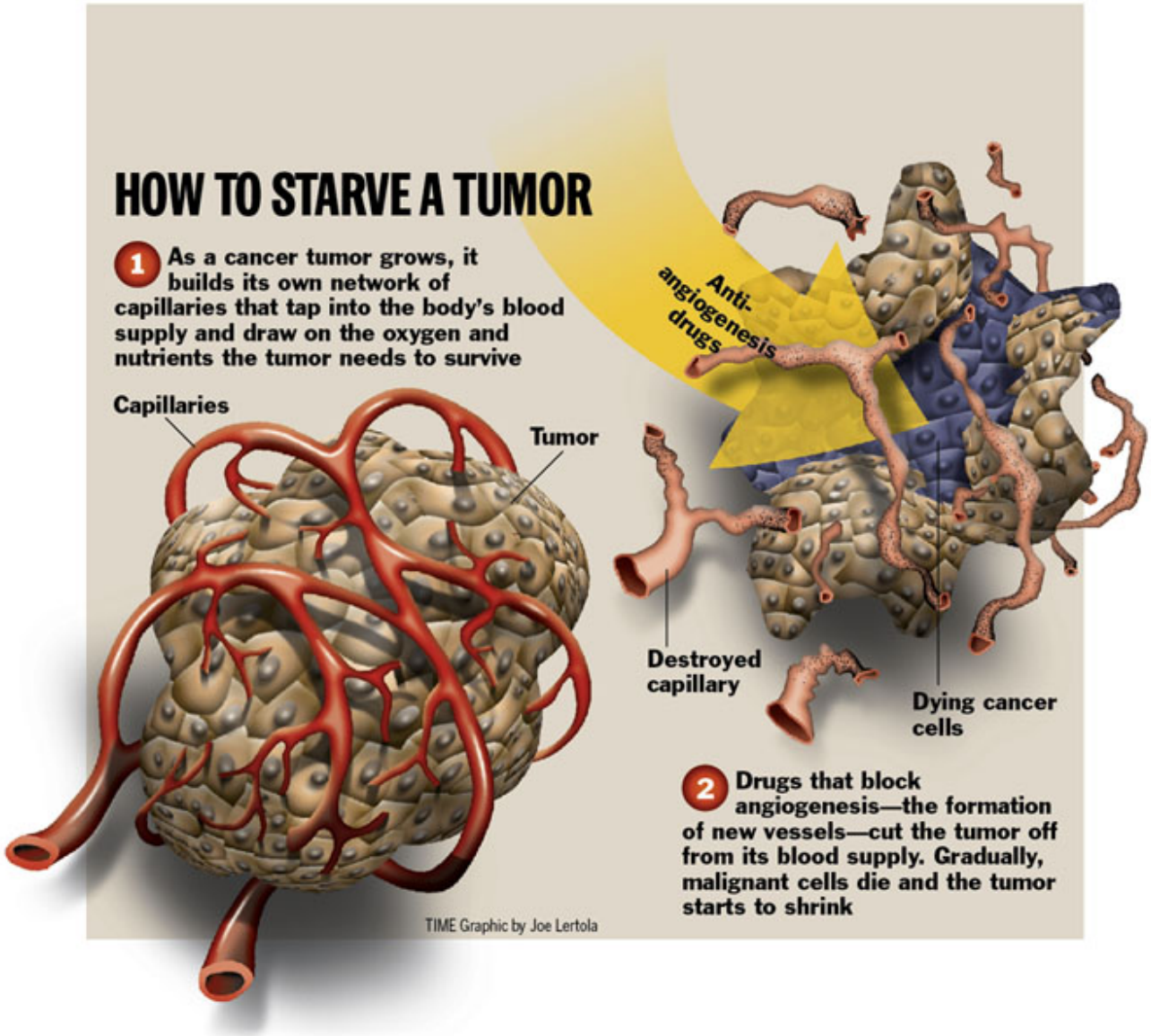
HOW TO STARVE A TUMOR
1 As a cancer tumor grows, it builds its own network of capillaries that tap into the body's blood supply and draw on the oxygen and nutrients the tumor needs to survive
Capillaries
Tumor
Anti-angiogenesis drugs
Destroyed capillary
Dying cancer cells
2 Drugs that block angiogenesis—the formation of new vessels—cut the tumor off from its blood supply. Gradually, malignant cells die and the tumor starts to shrink
TIME Graphic by Joe Lertola

Hepatic perfusion characteristics

increase / decrease with angiogenesis

- blood flow (BF) *microcirculation*
- blood volume (BV) *concentration*
- mean transit time (MTT)
- permeability surface-area product (PS) *capillary permeability and leakage (extracellular) space*
- hepatic arterial fraction (HAF) *extent of blood supply from aorta*

perfusion CT acquisition protocol

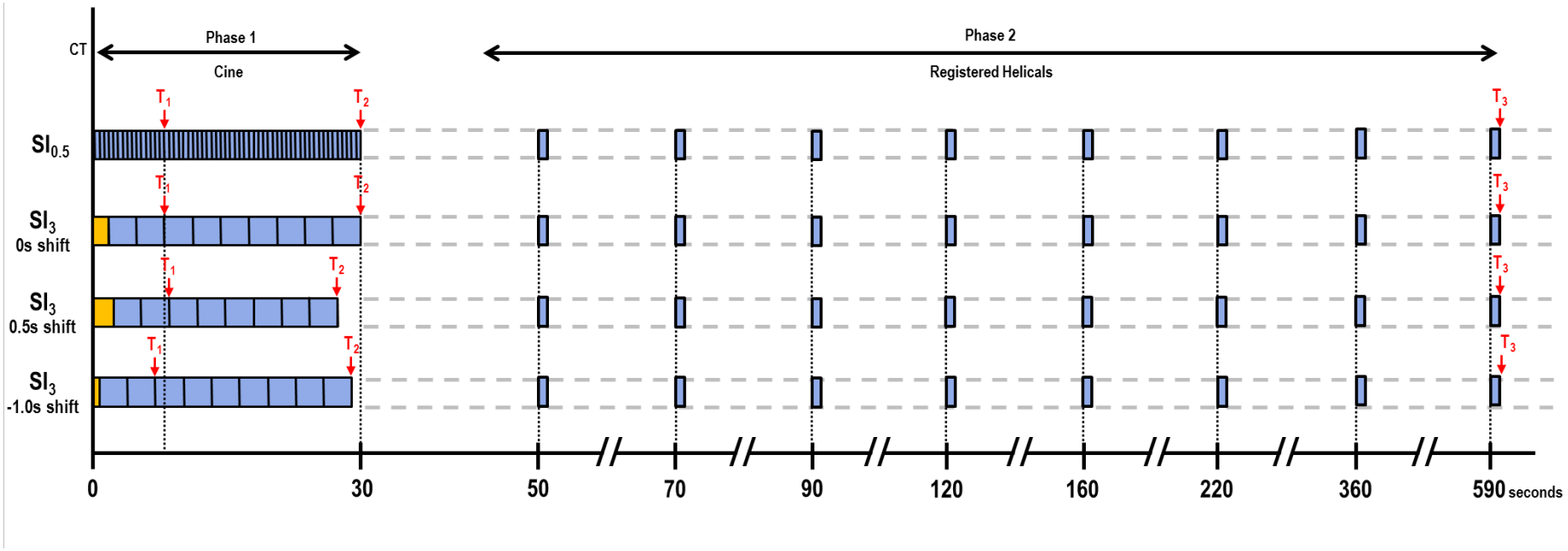

- Reference dataset: Phase 1, combined with 8 anatomically registered Phase 2 images.
  - T1, pre-enhancement setpoint
  - T2, last first phase setpoint
  - T3, last second phase (post-enhancement) setpoint

CT perfusion acquisition protocol

Recommendations pertaining to acquisition put forth in radiology literature used inappropriate statistical approaches!

- Goh, V. et al. (2005), *J Comput Assist Tomogr*
- Kambadakone, A. et al. (2011), *Eur Radiol*

Stable acquisition duration 30-45 secs was "inferred":

- t-tests between CTp values obtained at discrete acquisition durations using a traditional hypothesis testing framework
- stability was concluded in the absence of significant differences for tests between successive scans
- conclusions were also based on measures of linear dependence between pairs of intra-patient observations at successive scans

CT perfusion acquisition protocol

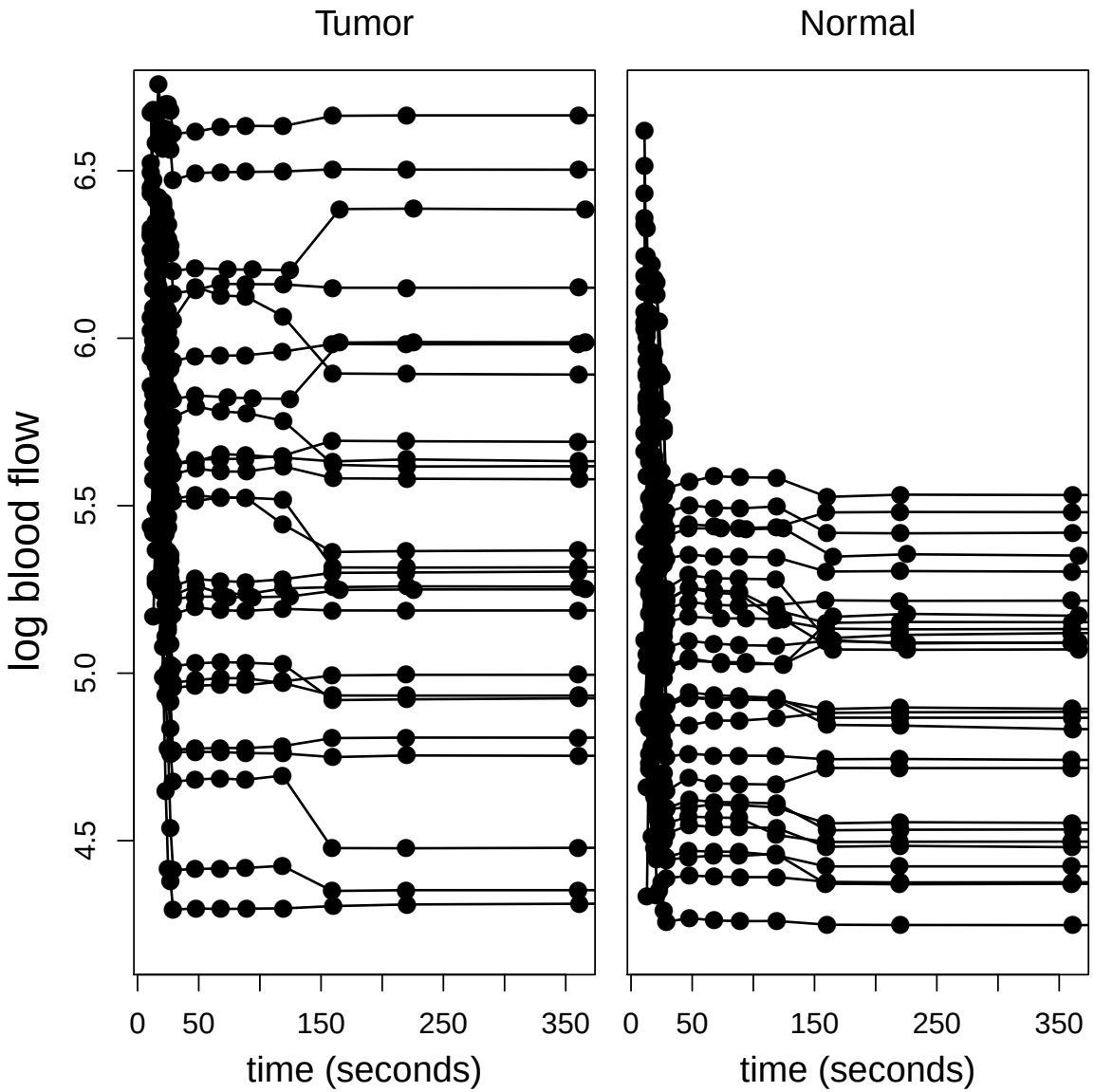

CT perfusion acquisition duration

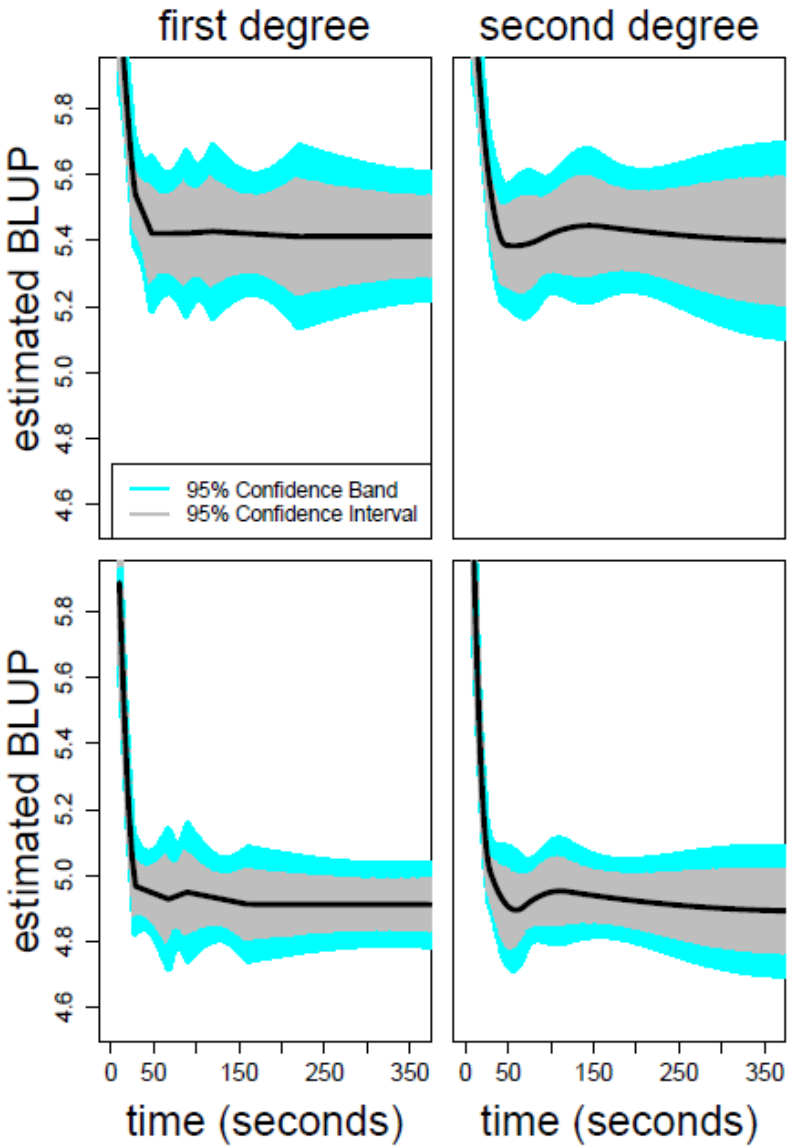

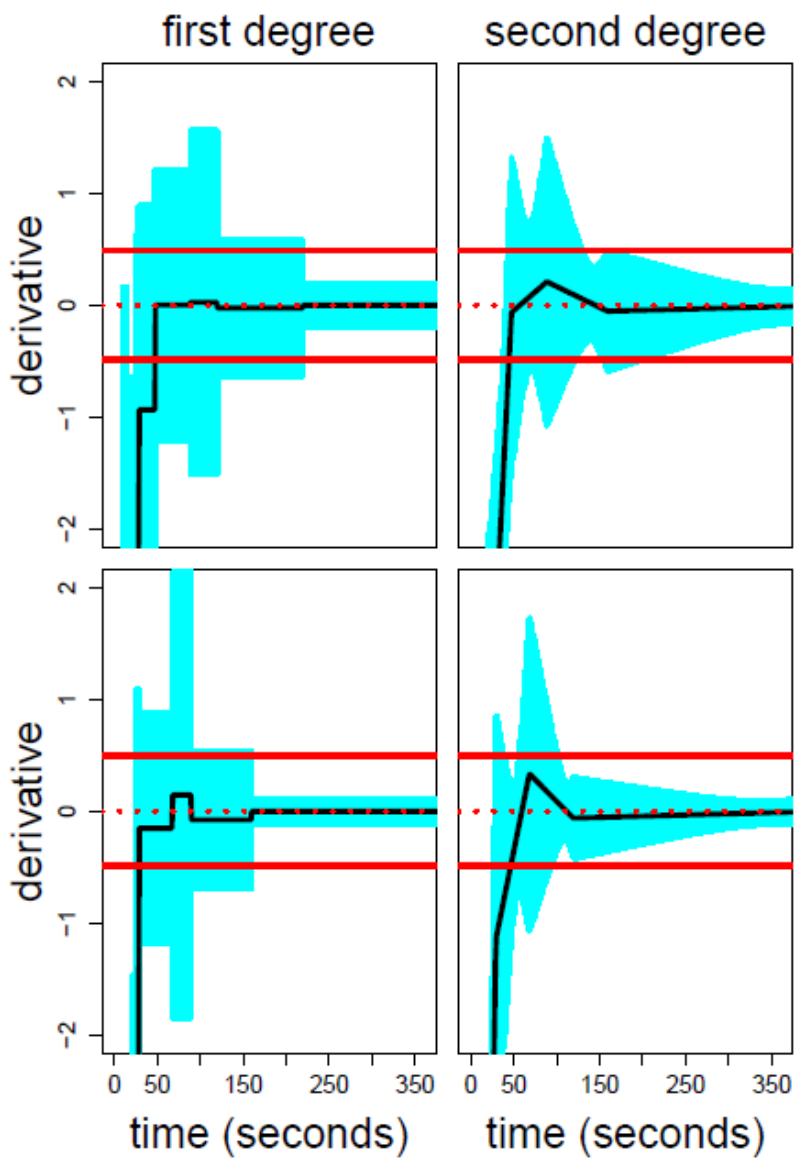

CT perfusion acquisition duration (cont)

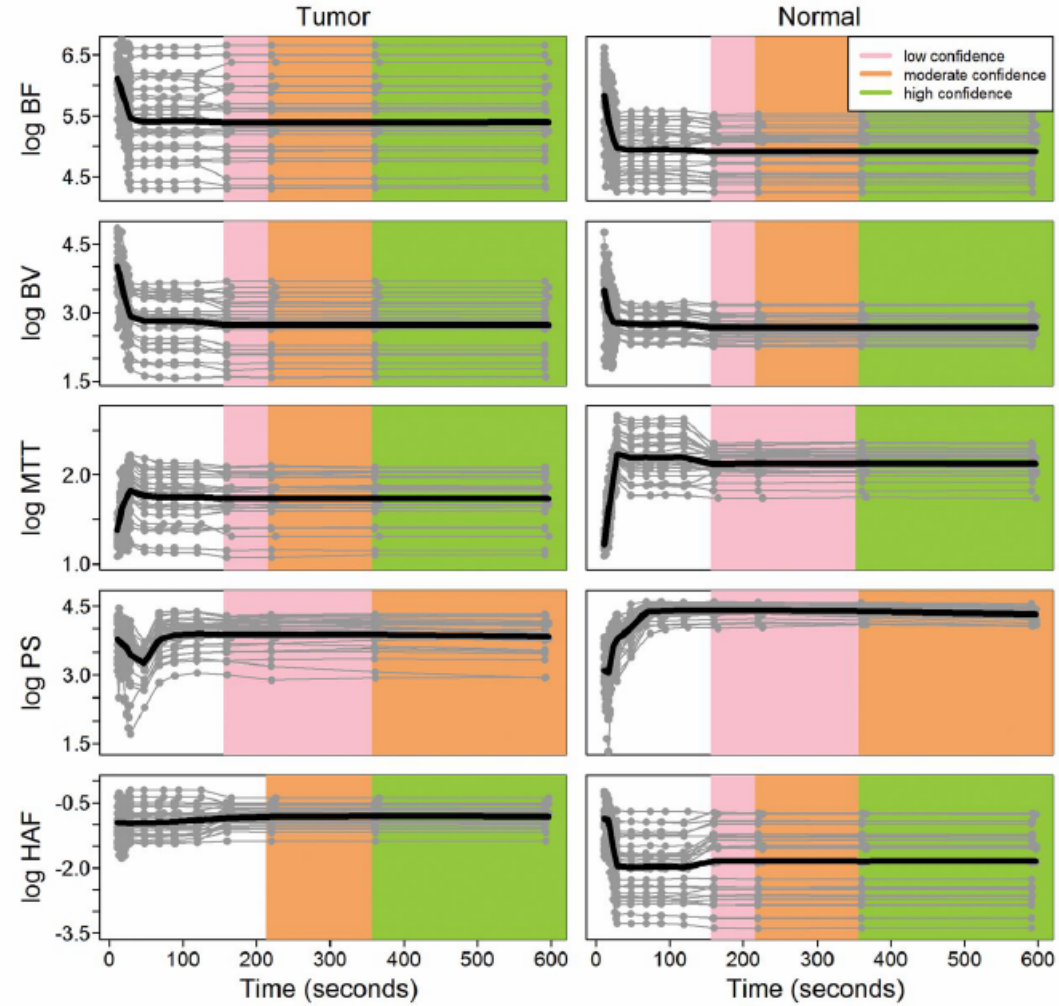

Ng C S et al. Radiology doi:10.1148/radiol.13122708

Radiology

CT perfusion acquisition protocol

Our recommended protocol for CTp acquisition in liver

- Ng C., Hobbs, B., et al. (2013), Metastases to the liver from neuroendocrine tumors: Effect of duration of scan acquisition on CT perfusion values, *Radiology*
- Ng, C., Hobbs, B., et al. (2014), Effect of sampling frequency on perfusion values in CT perfusion of liver tumors and normal liver, *J Comput Assist Tomogr*
- Ng, C., Hobbs, B., et al. (2014), Effect of pre-enhancement set-point on CT perfusion values in normal liver and metastases to the liver from neuroendocrine tumors, *J Comput Assist Tomogr*
- Hobbs B, and Ng C. (2015). Inferring stable acquisition durations for applications of perfusion imaging in oncology, *Cancer Informatics*

Diagnostic tool enabling quantitative evaluation

Unenhanced axial CT scan $\Rightarrow$ 5 perfusion characteristics over 4 scans

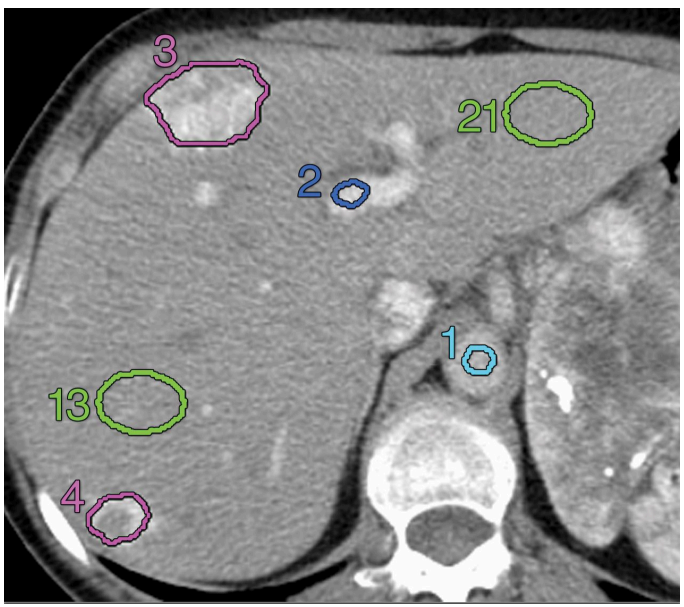

$\Rightarrow$

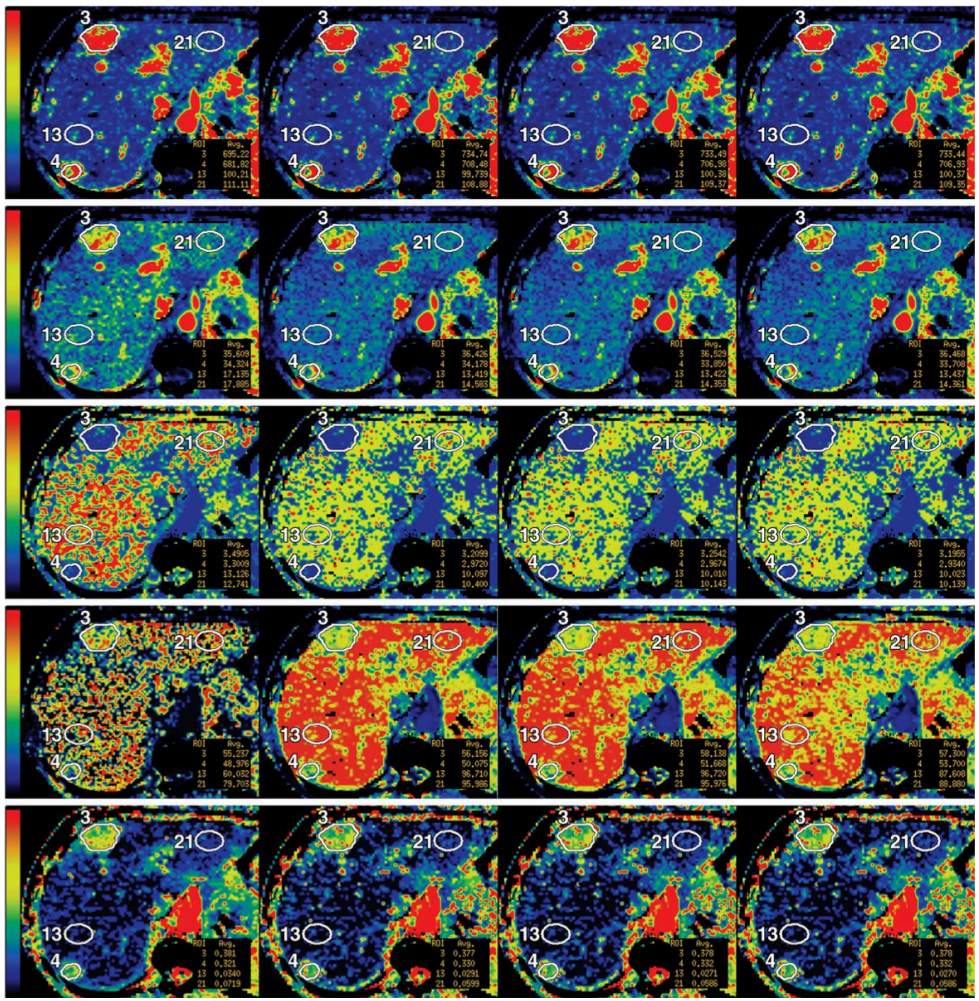

Current practice in diagnostic radiology

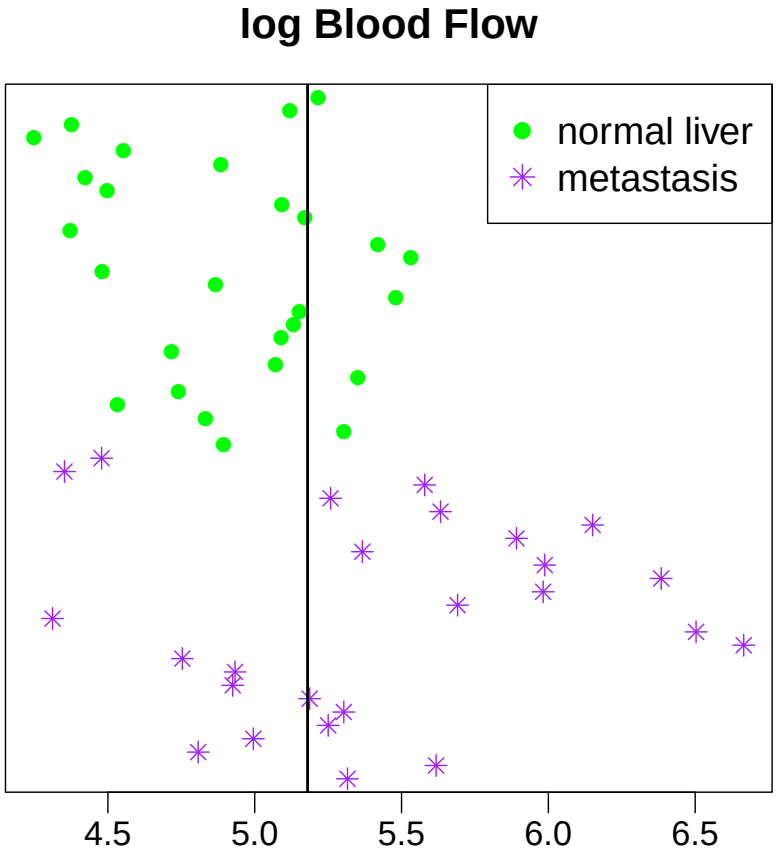

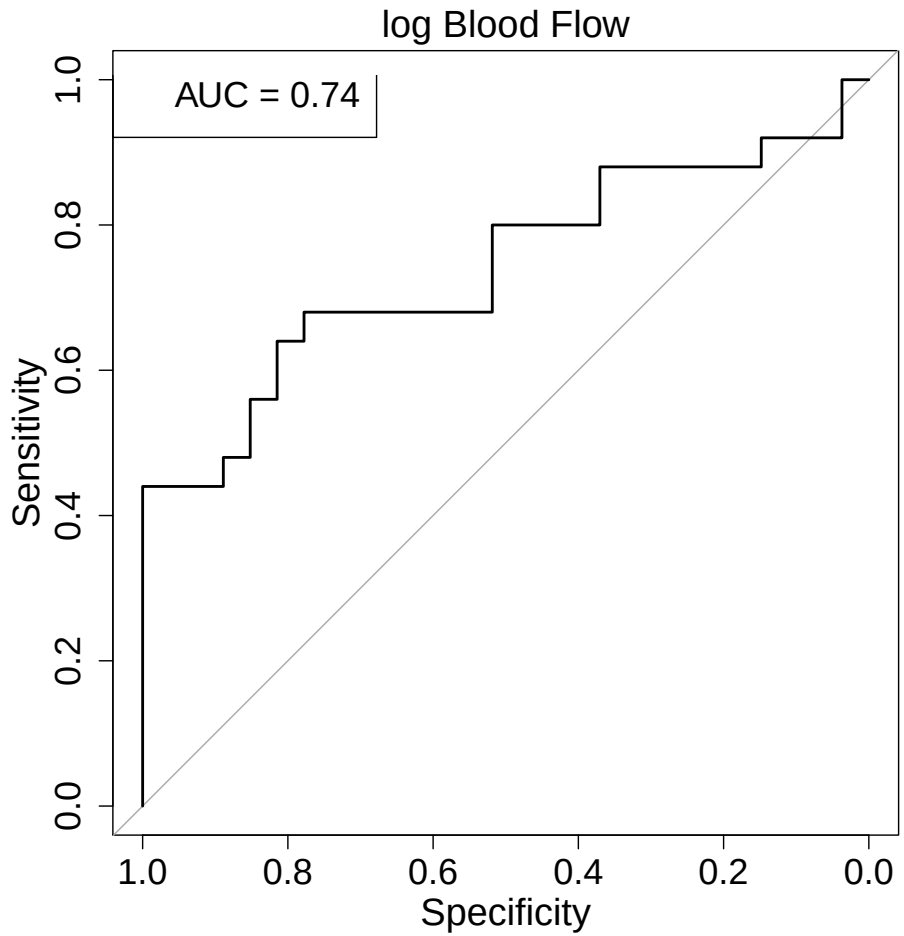

∗ tumor ○ normal

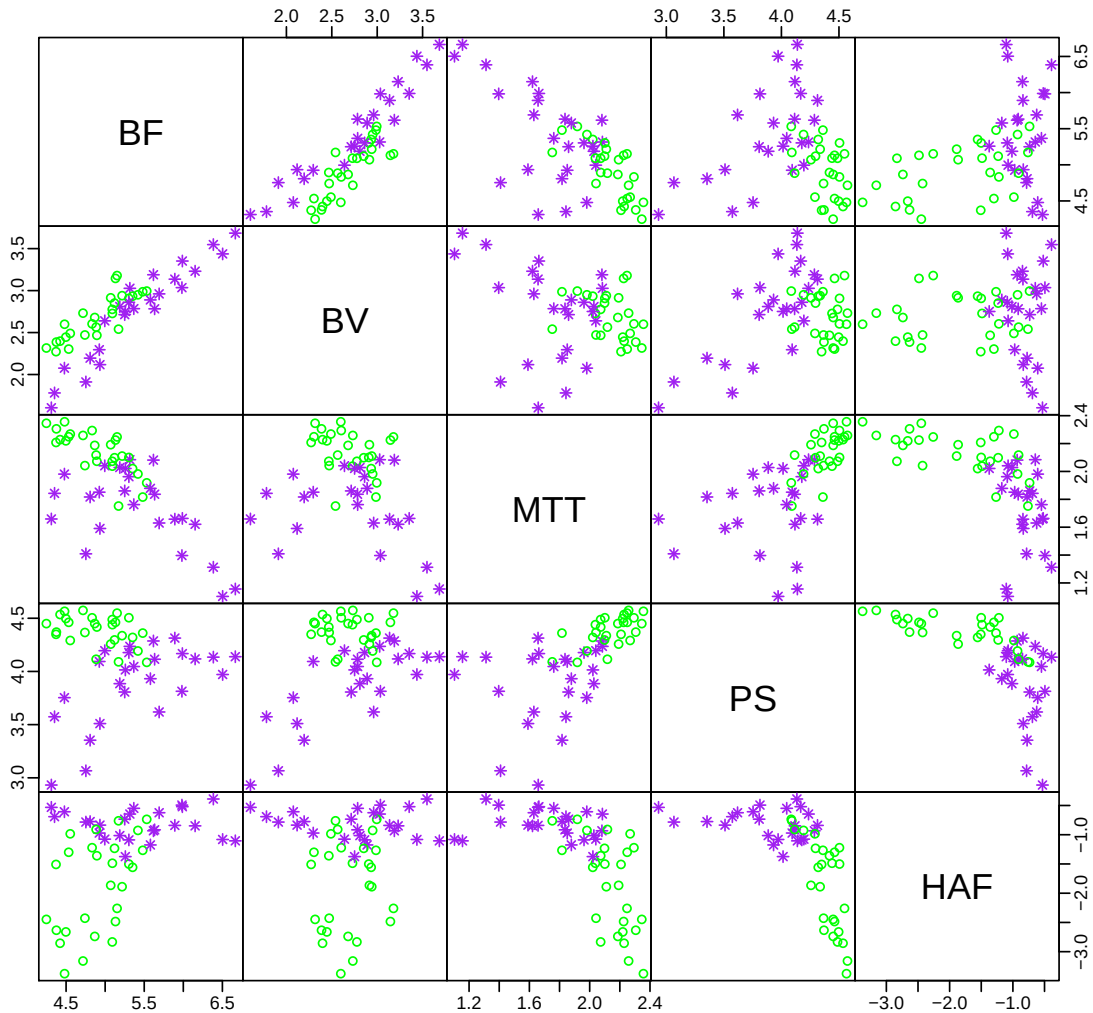

- Perfusion characteristics are correlated.
- The correlation is heterogeneous across tissue types.

Approaches that leverage between feature dependence

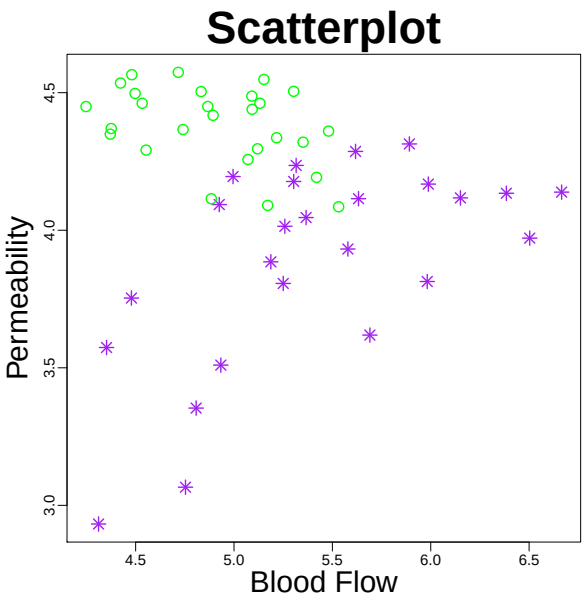

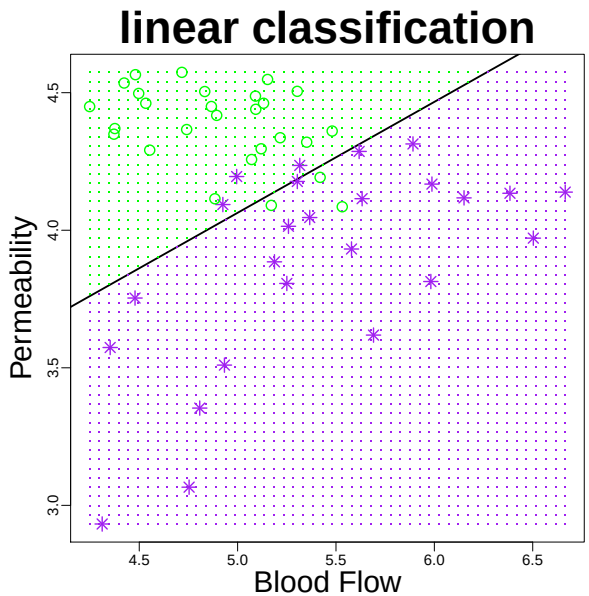

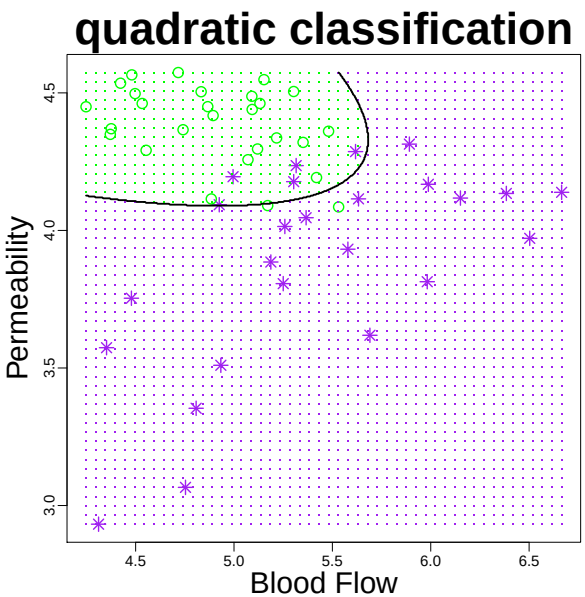

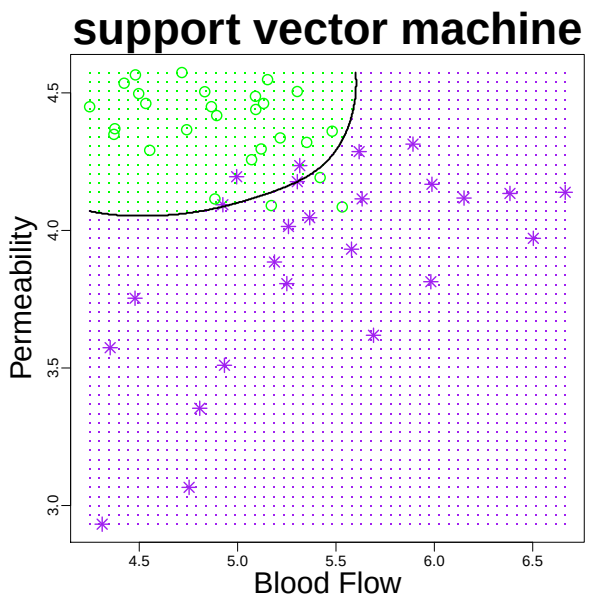

Class assignments are evaluated independently

Inter-Region Correlation

patient 8

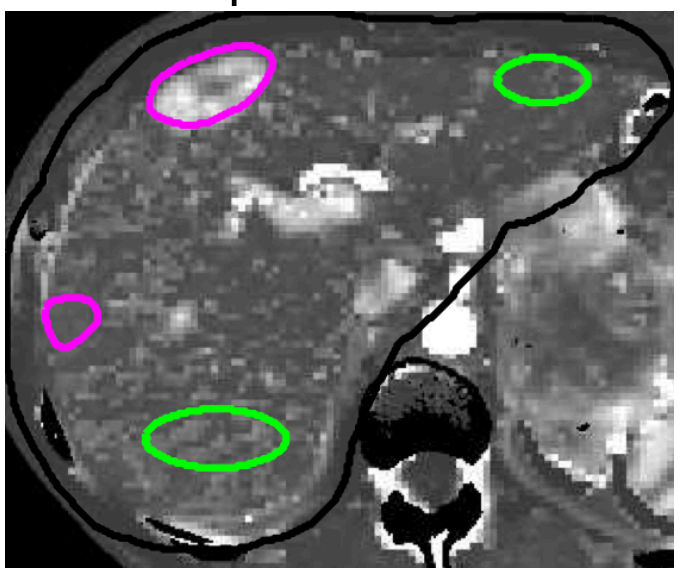

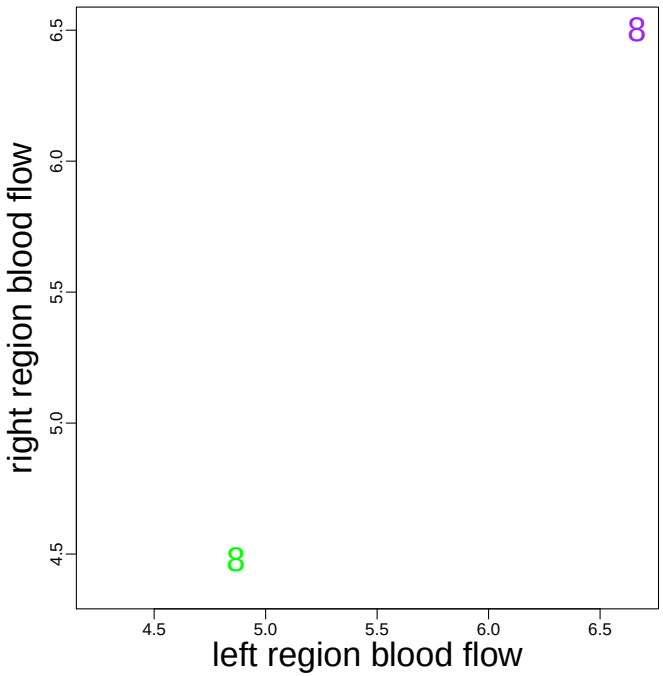

Inter-Region Correlation

patient 8

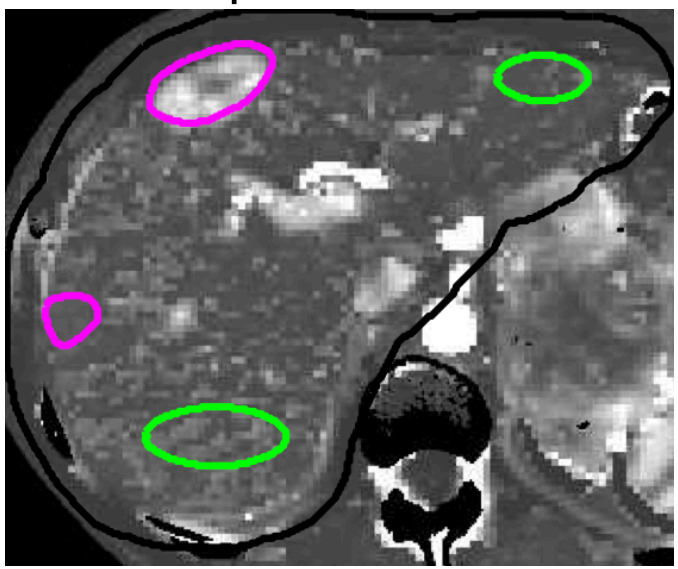

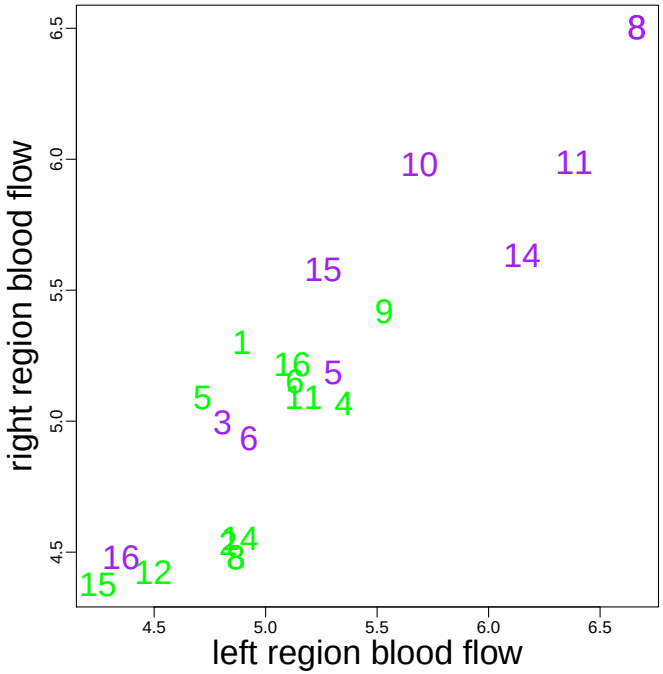

Sample Correlation for neighboring regions of the same tissue type

BF	BV	MTT	PS	HAF
0.88	0.86	0.72	0.71	0.90

Simultaneous Classification for ROI level inference

	region 1	region 2	region 3	region 4
1	tumor	tumor	tumor	tumor
2	normal	tumor	tumor	tumor
3	tumor	normal	tumor	tumor
⋮	⋮	⋮	⋮	⋮
6	normal	normal	tumor	tumor
7	tumor	normal	normal	tumor
⋮	⋮	⋮	⋮	⋮
16	normal	normal	normal	normal

Wang Y, Hobbs, BP, Hu J, Ng C, Do K, "Predictive Classification of Correlated Targets with Application to Detection of Metastatic Cancer using Functional CT Imaging," *Biometrics*, 2015.

Model

Notation

- z: tissue type; m: number of features
- i: patient index, $i = 1, \ldots, N$; j: region index, $j = 1, \ldots, n_i$
- $\boldsymbol{y}_{ij}$: measurement for the patient i region j
- s_{ij}: region location

Distribution:

- $vec(\boldsymbol{Y}_i^z) \sim N(\mathbf{1}_{n_i^z} \otimes \boldsymbol{\mu}_z, \boldsymbol{\Psi}_i^z \otimes \boldsymbol{\Sigma}_z)$
- Intra-region:
  - Mean: $\boldsymbol{\mu}_z = \mathbb{E}[\boldsymbol{y}_{ij}|Z = z]$
  - Covariance: $\boldsymbol{\Sigma}_z = \text{cov}(\boldsymbol{y}_{ij}|Z = z)$
- Inter-region:
  - Independence across patients
  - Independence across tissue classes
  - Within the same patient and the same tissue class

$$\text{cov}(\boldsymbol{y}_{ij}, \boldsymbol{y}_{ij'}) = \psi(s_{ij}, s_{ij'})\boldsymbol{\Sigma}_z$$

Model

Notation

- z: tissue type; m: number of features
- i: patient index, $i = 1, \ldots, N$; j: region index, $j = 1, \ldots, n_i$
- $\boldsymbol{y}_{ij}$: measurement for the patient i region j
- s_{ij}: region location

Distribution:

- $vec(\boldsymbol{Y}_i^z) \sim N(\mathbf{1}_{n_i^z} \otimes \boldsymbol{\mu}_z, \boldsymbol{\Psi}_i^z \otimes \boldsymbol{\Sigma}_z)$
- Intra-region:
  - Mean: $\boldsymbol{\mu}_z = \mathbb{E}[\boldsymbol{y}_{ij}|Z = z]$
  - Covariance: $\boldsymbol{\Sigma}_z = \text{cov}(\boldsymbol{y}_{ij}|Z = z)$
- Inter-region:
  - Independence across patients
  - Independence across tissue classes
  - Within the same patient and the same tissue class

$$\text{cov}(\boldsymbol{y}_{ij}, \boldsymbol{y}_{ij'}) = \psi(s_{ij}, s_{ij'})\boldsymbol{\Sigma}_z$$

Note: separable correlation between biomarker and location

Model

Inter-region correlation:

- Independence across patients
- Independence across tissue classes
- Within the same patient and the same tissue class

$$\mathrm{cov}(\boldsymbol{y}_{ij}, \boldsymbol{y}_{ij'}) = \psi(s_{ij}, s_{ij'})\boldsymbol{\Sigma}_z$$

- For features from identical class we assume:
- Inter-region correlation for identical feature $= \psi(s_{ij}, s_{ij'})$
- Inter-region cross-correlations $=$ intra-region cross-correlation scaled by $\psi(s_{ij}, s_{ij'})$
- separability reduces the degrees of freedom in the covariance from $\frac{1}{2}n_i^z m(n_i^z m + 1)$ to $\frac{1}{2}n_i^z(n_i^z + 1) + \frac{1}{2}m(m + 1)$

Inter-Region Correlation Models

- Compound symmetry

$$\psi(s_{ij}, s_{ij'}; \phi) \equiv \phi$$

- Spatial dependence
  - Exponential:

$$\psi(s_{ij}, s_{ij'}; \phi) = \exp\{-\frac{d}{\phi}\}, \quad d = \text{dist}(s_{ij}, s_{ij'})$$

  - Spherical:

$$\psi(s_{ij}, s_{ij'}; \phi) = \begin{cases} 1 - \frac{2}{\pi}\left(\frac{d}{\phi}\sqrt{1-(\frac{d}{\phi})^2} + \sin^{-1}\frac{d}{\phi}\right) & d < \phi \\ 0 & d \geq \phi \end{cases}$$

- General structure
  - Anisotropic models, etc.

Simultaneous Bayesian Classification: ROI inference

- Data: train $\mathcal{Y}$, test $\mathcal{Y}_0$
- The simultaneous Bayesian classification rule is

$$\widehat{\boldsymbol{d}}_0 = \arg\min_{\boldsymbol{d}\in\mathcal{D}} \sum_{\boldsymbol{d}_k\in\mathcal{D}} L_\alpha(\boldsymbol{d}_k, \boldsymbol{d}) p(\boldsymbol{d}_k|\mathcal{Y}_0, \mathcal{Y})$$

  - $p(\boldsymbol{d}_k|\mathcal{Y}_0, \mathcal{Y})$: the joint posterior classification probability
  - $L_\alpha(\boldsymbol{d}_k, \boldsymbol{d})$: the joint weighted 0-1 loss:

$$L_\alpha(\boldsymbol{d}_k, \boldsymbol{d}) = \sum_k \{\alpha\{\text{false negative}\} + (1-\alpha)\{\text{false positive}\}\}$$

  - $\mathcal{D}$: the set of all the possible class configurations
  - requires a prior probability for each possible configurations

$$\Pr(\boldsymbol{z}_{N+1} = \boldsymbol{d}_k) = p^l(1-p)^{n_{N+1}-l},$$

    where l = number of tumor ROIs given by $\boldsymbol{d}_k$.
  - Hyperparameter p is fixed at the estimated rate of tumor incidence in the presence of the training data.

Simultaneous Bayesian Classification: ROI inference

- Data: train $\mathcal{Y}$, test $\mathcal{Y}_0$
- The simultaneous Bayesian classification rule is

$$\widehat{\boldsymbol{d}}_0 = \arg\min_{\boldsymbol{d}\in\mathcal{D}} \sum_{\boldsymbol{d}_k\in\mathcal{D}} L_\alpha(\boldsymbol{d}_k, \boldsymbol{d}) p(\boldsymbol{d}_k|\mathcal{Y}_0, \mathcal{Y})$$

  - $p(\boldsymbol{d}_k|\mathcal{Y}_0, \mathcal{Y})$: the joint posterior classification probability
  - $L_\alpha(\boldsymbol{d}_k, \boldsymbol{d})$: the joint weighted 0-1 loss:

$$L_\alpha(\boldsymbol{d}_k, \boldsymbol{d}) = \sum_k \{\alpha\{\text{false negative}\} + (1-\alpha)\{\text{false positive}\}\}$$

  - $\mathcal{D}$: the set of all the possible class configurations
  - requires a prior probability for each possible configurations

$$\Pr(\boldsymbol{z}_{N+1} = \boldsymbol{d}_k) = p^l(1-p)^{n_{N+1}-l},$$

    where l = number of tumor ROIs given by $\boldsymbol{d}_k$.
  - Hyperparameter p is fixed at the estimated rate of tumor incidence in the presence of the training data.

Maximum *a posteriori* classifier $\neq$ Minimum risk classifier *Bayesian*

Detection of ROIs with Metastases using Perfusion Biomarkers

- True positive rate (TPR): proportion of correctly identified tumor
- False positive rate (FPR): proportion of falsely identified normal

		method	TPR	FPR
Conventional		Bayesian quadratic	0.76	0.18
		Support vector machine	0.88	0.19
Simultaneous	(1)	$\alpha = 0.5$ (equal cost)	0.96	0.07
		$\alpha = 0.8$ (prefer FP)	0.96	0.11
	(2)	$\alpha = 0.5$ (equal cost)	0.96	0.04
		$\alpha = 0.8$ (prefer FP)	1.00	0.19

(1) compound symmetry; (2) exponential decay

Simulation Study

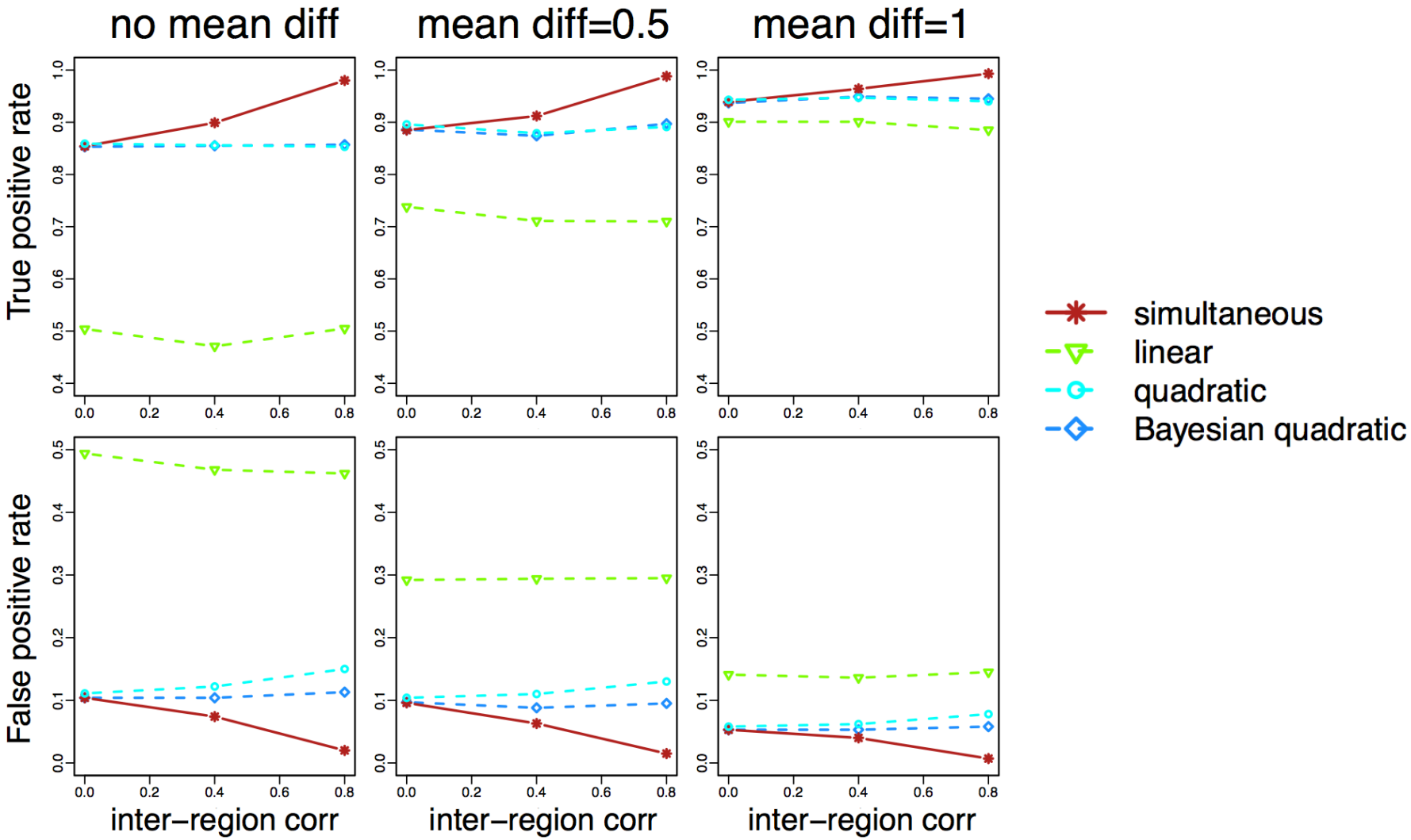

Voxel-level Posterior Probability maps from integration of perfusion features

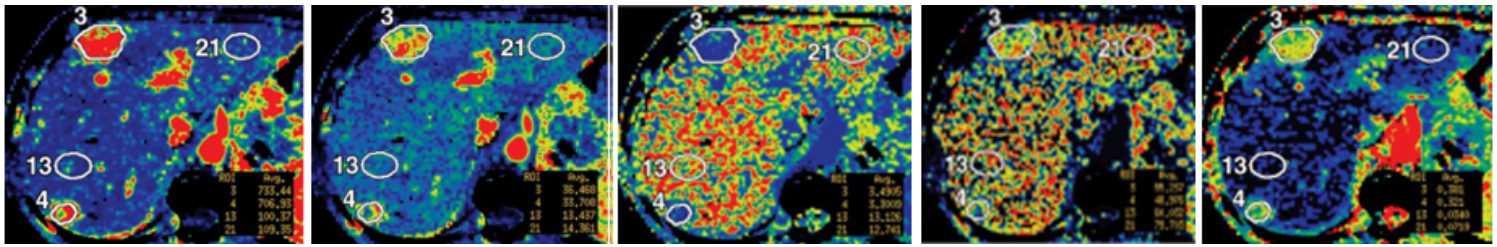

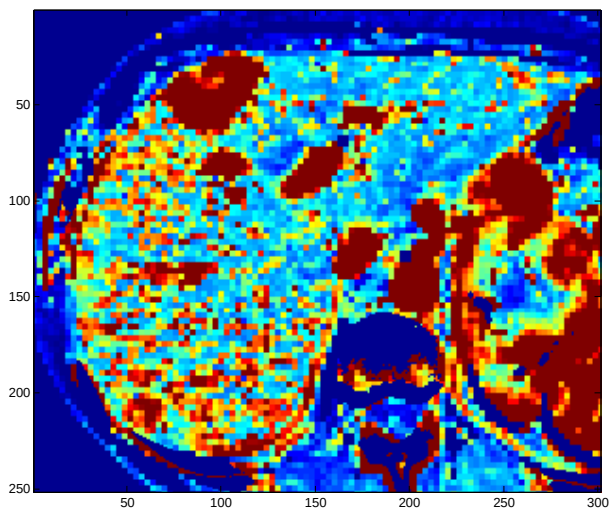

Gaussian Process Framework

Capturing Spatial Dependence among the perfusion features at voxel level:

- Option 1: Assume *a priori* voxel-wise Independence with application of 3D smoothing to resulting posterior probability maps
- Option 2: Induce Dependent Class Assignments (Markov random field)

$$\Pr(\boldsymbol{z}_{N+1}) \propto c(\beta) \exp\left\{\beta \sum_{i \sim i^*} w_{i,j} I(z_i = z_{i^*})\right\}$$

with pre-specified "network" or neighborhood structure $i \sim i^*$

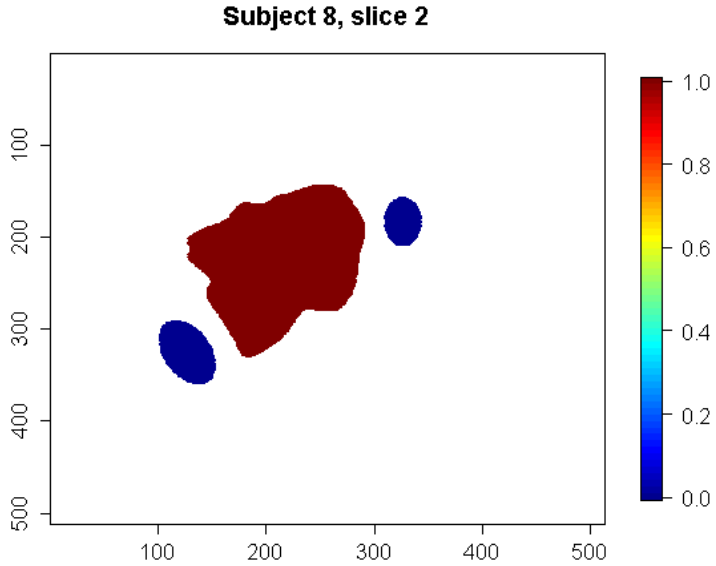
Subject 8, slice 2
100
200
300
400
500
1.0
0.8
0.6
0.4
0.2
0.0

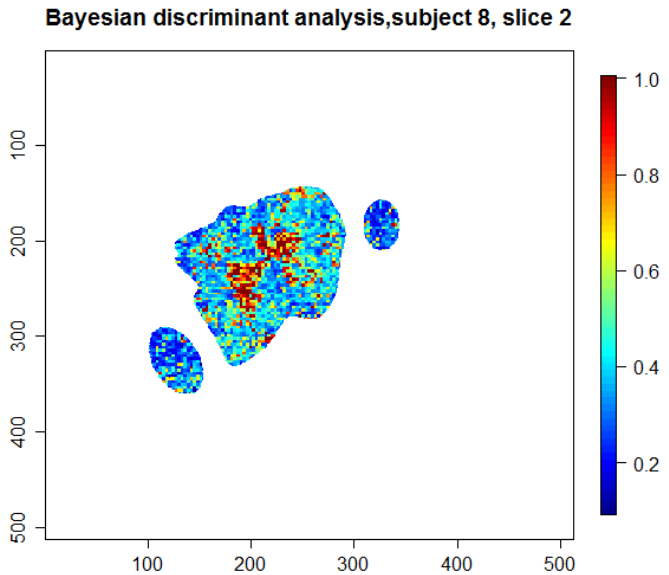
Bayesian discriminant analysis,subject 8, slice 2
100
200
300
400
500
1.0
0.8
0.6
0.4
0.2

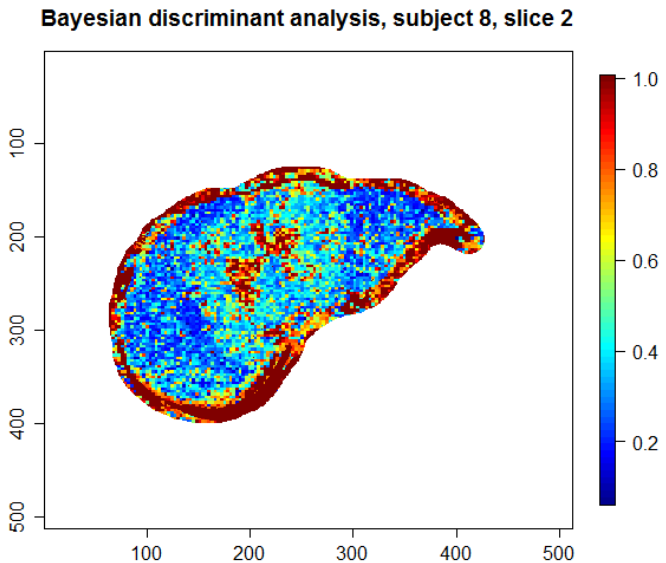
Bayesian discriminant analysis, subject 8, slice 2
100
200
300
400
500
1.0
0.8
0.6
0.4
0.2

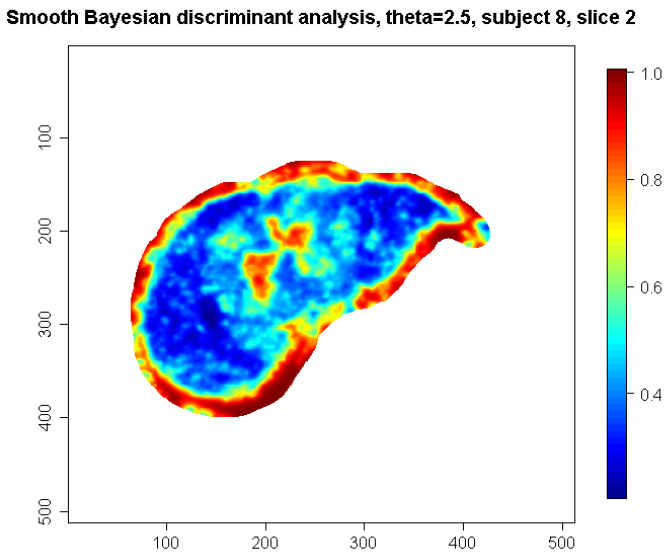
Smooth Bayesian discriminant analysis, theta=2.5, subject 8, slice 2
100
200
300
400
500
1.0
0.8
0.6
0.4

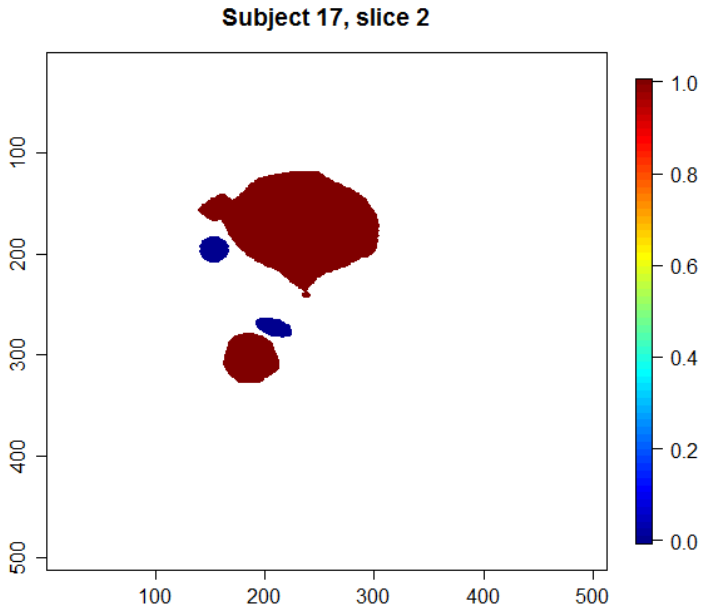
Subject 17, slice 2
100
200
300
400
500
1.0
0.8
0.6
0.4
0.2
0.0

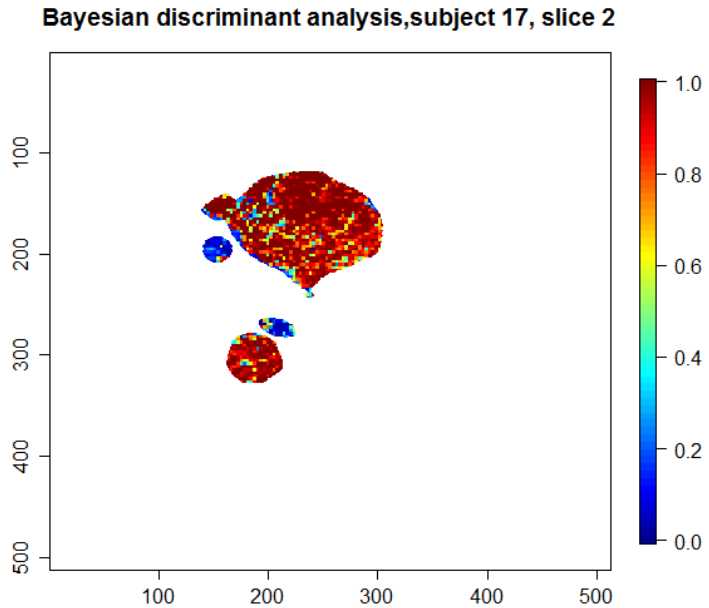
Bayesian discriminant analysis,subject 17, slice 2
100
200
300
400
500
1.0
0.8
0.6
0.4
0.2
0.0

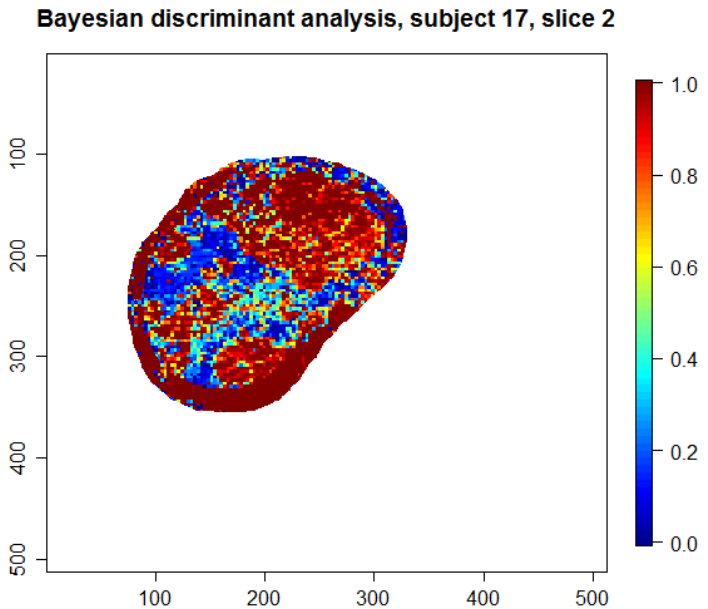
Bayesian discriminant analysis, subject 17, slice 2
100
200
300
400
500
1.0
0.8
0.6
0.4
0.2
0.0

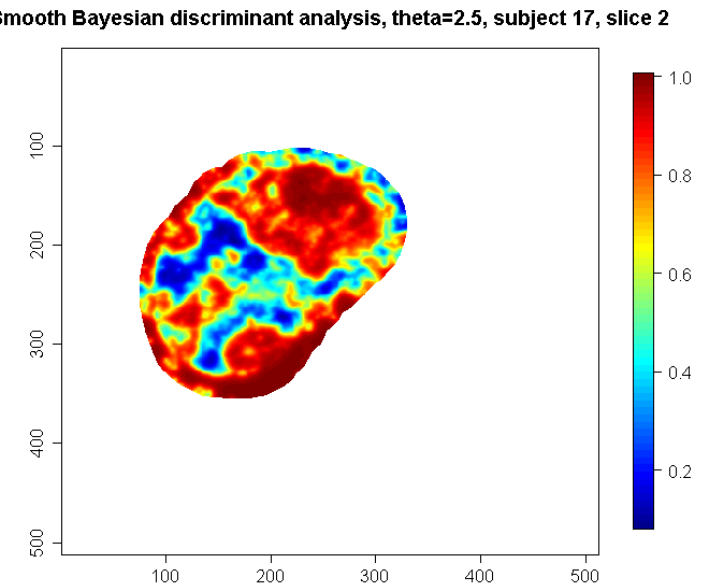
Smooth Bayesian discriminant analysis, theta=2.5, subject 17, slice 2
100
200
300
400
500
1.0
0.8
0.6
0.4
0.2

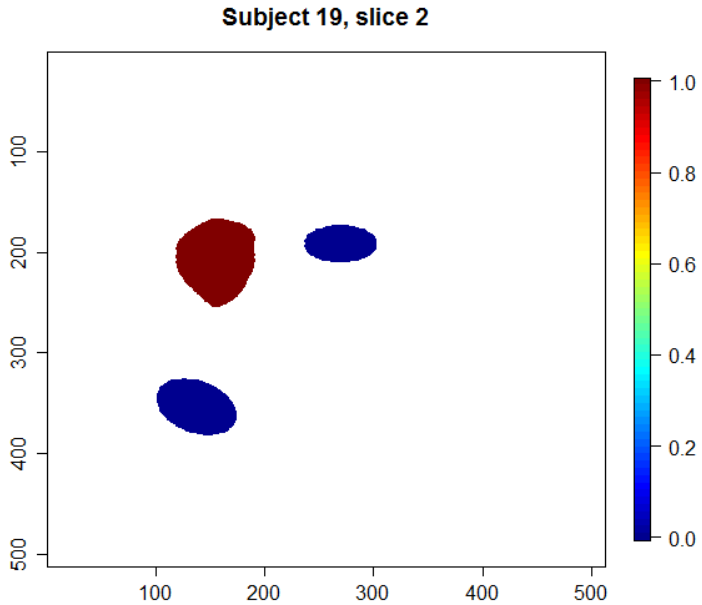
Subject 19, slice 2
100
200
300
400
500
1.0
0.8
0.6
0.4
0.2
0.0

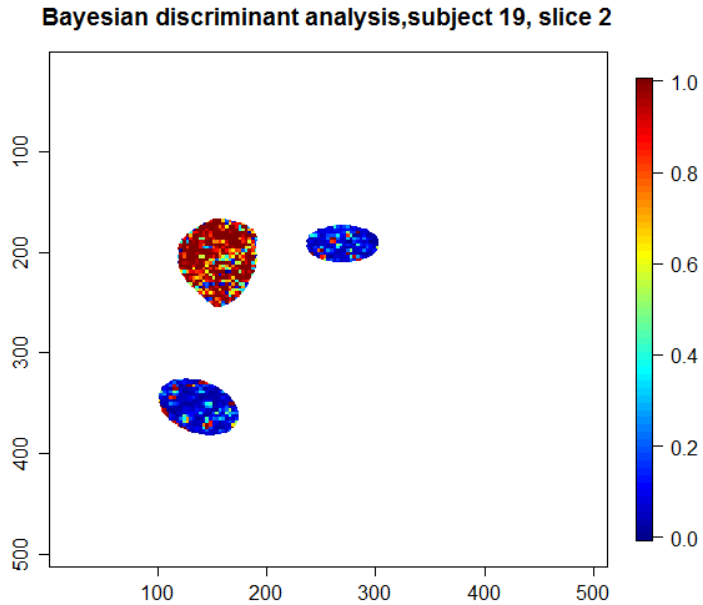
Bayesian discriminant analysis,subject 19, slice 2
100
200
300
400
500
1.0
0.8
0.6
0.4
0.2
0.0

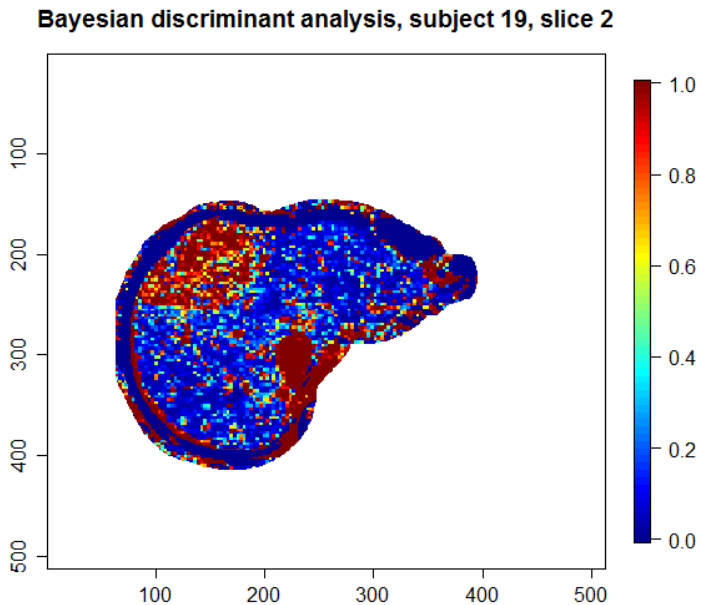
Bayesian discriminant analysis, subject 19, slice 2
100
200
300
400
500
1.0
0.8
0.6
0.4
0.2
0.0

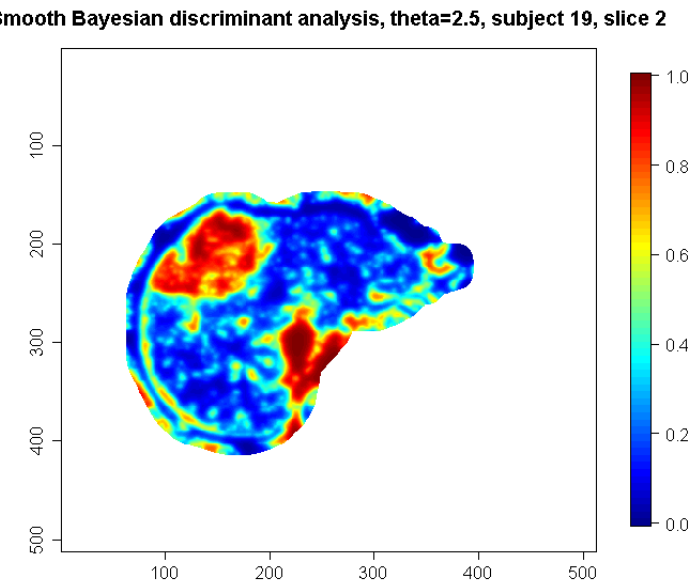
Smooth Bayesian discriminant analysis, theta=2.5, subject 19, slice 2
100
200
300
400
500
1.0
0.8
0.6
0.4
0.2
0.0

Bayesian Nonparametric Voxel-level Inference

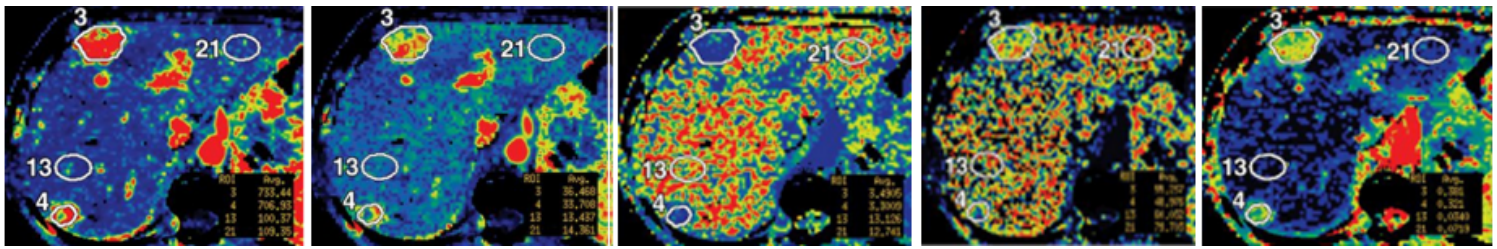

Identify perfusion "signatures"

- flexibility for describing inter-feature dependence through clustering methods
- integrate voxel-level similarity measure into Bayesian predictive framework

Perfusion "signatures"

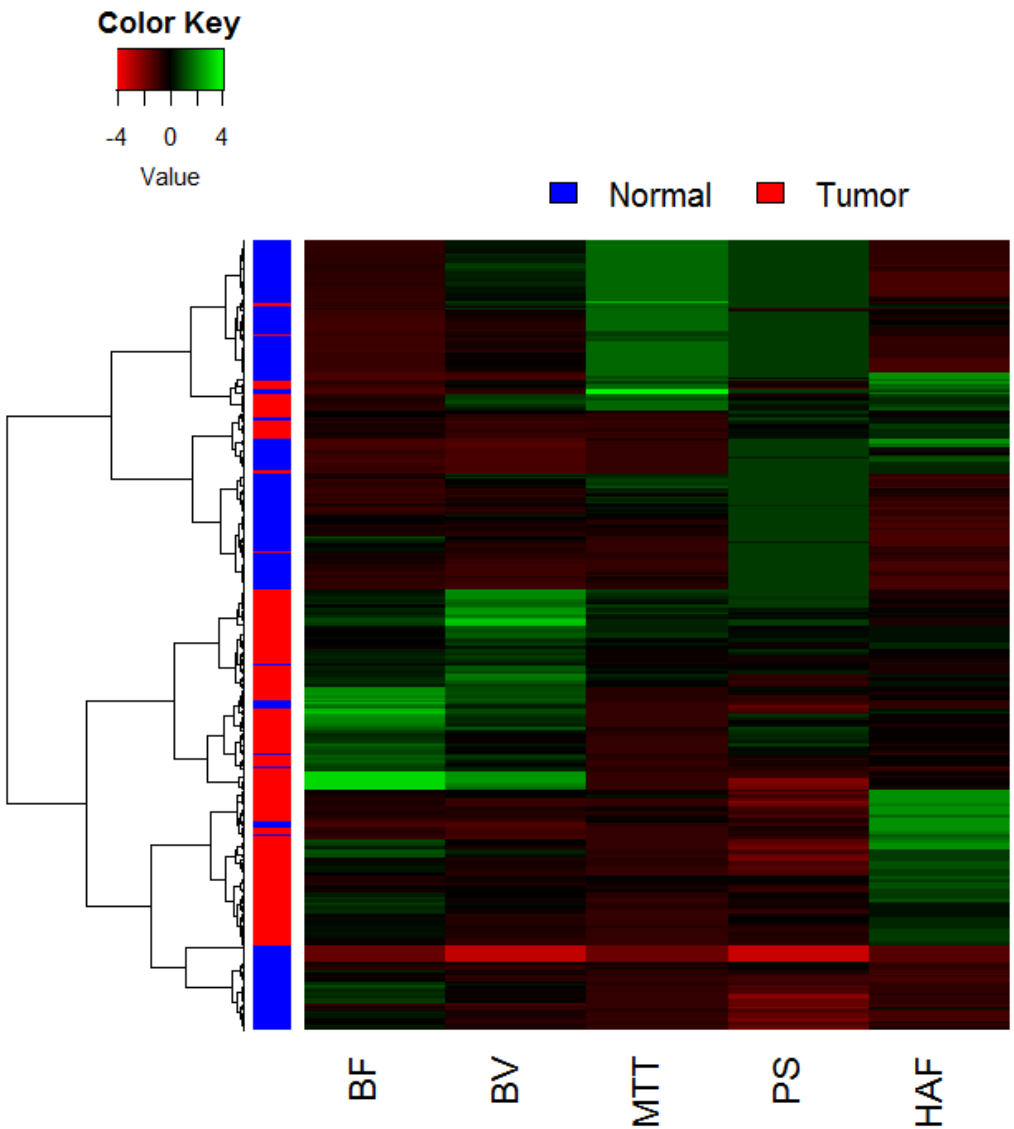

Using 5 latent clusters

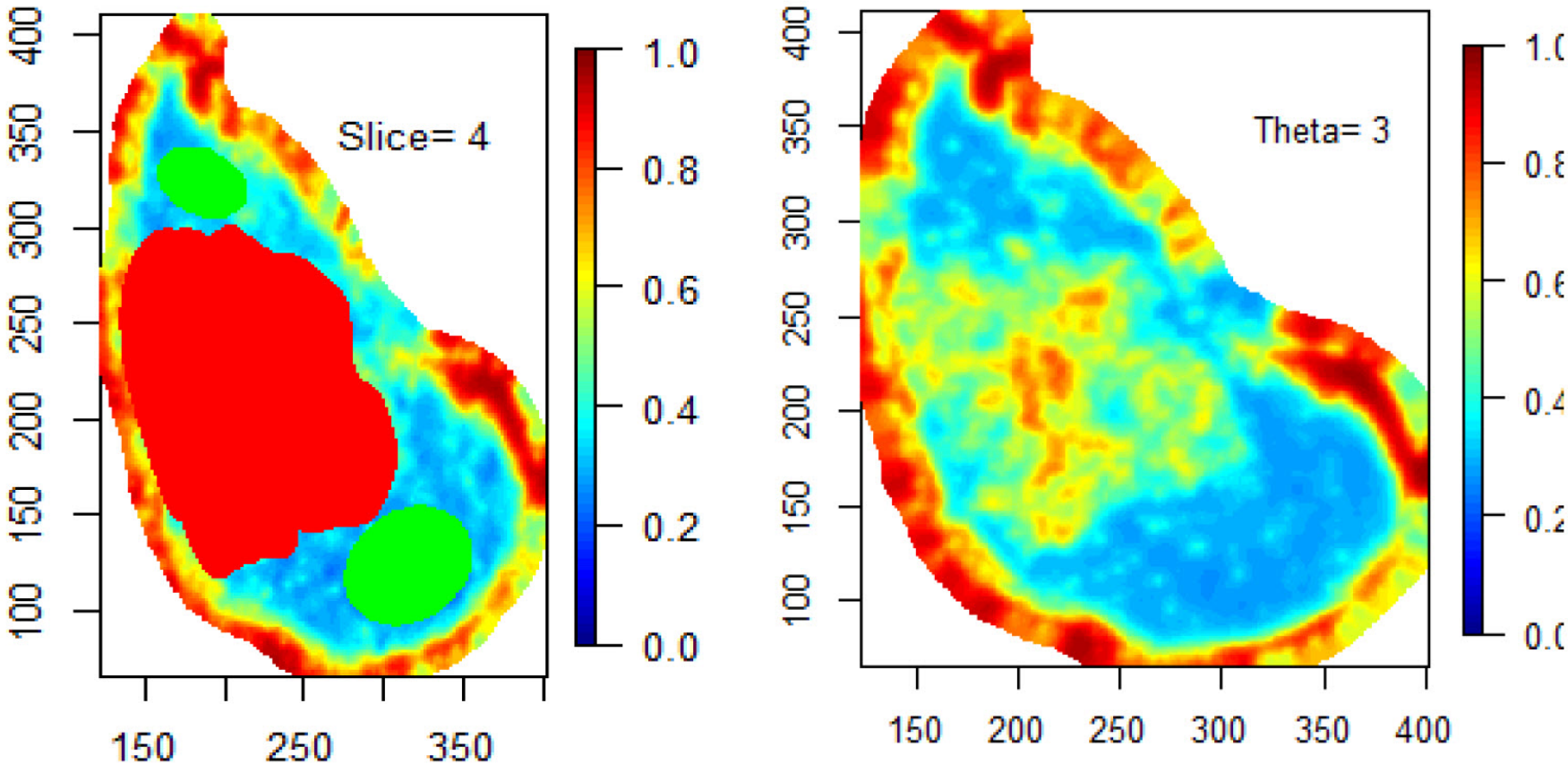

One slice of voxel-wise posterior probability map

Using 5 latent clusters

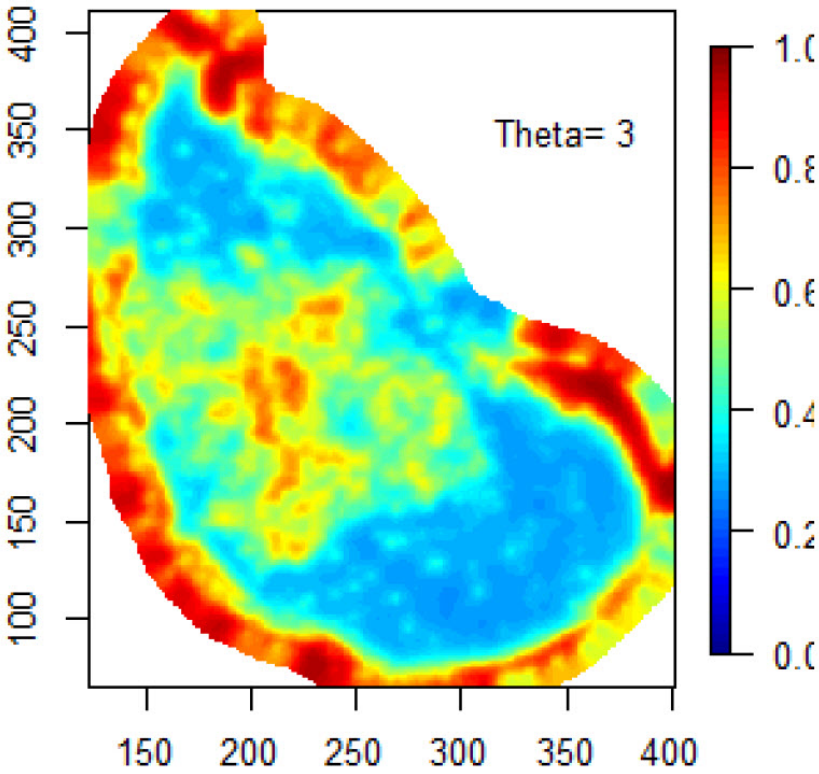

Posterior Probability Map

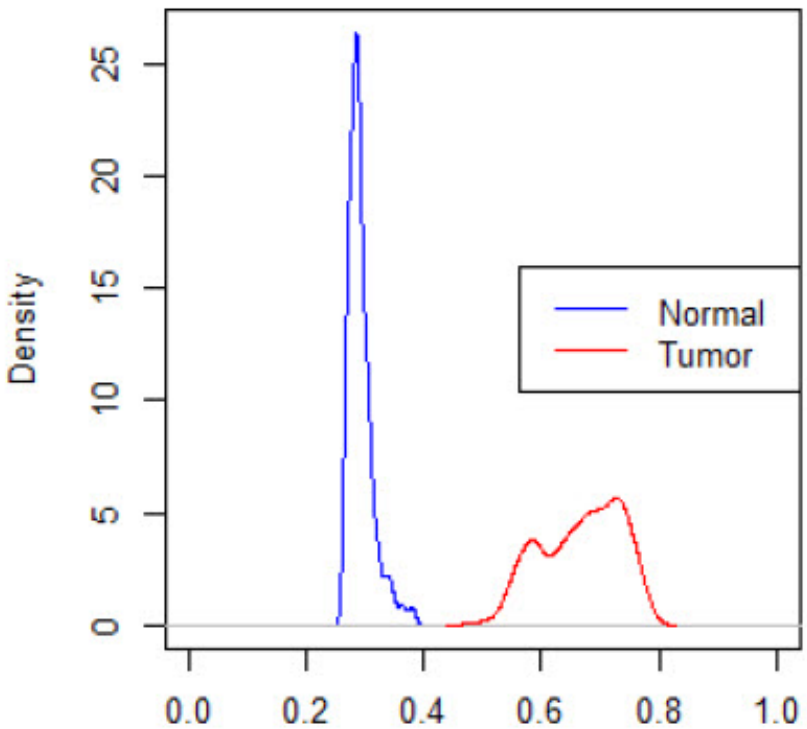

Distributions of smoothed posterior probabilities among training voxels

Using 5 latent clusters

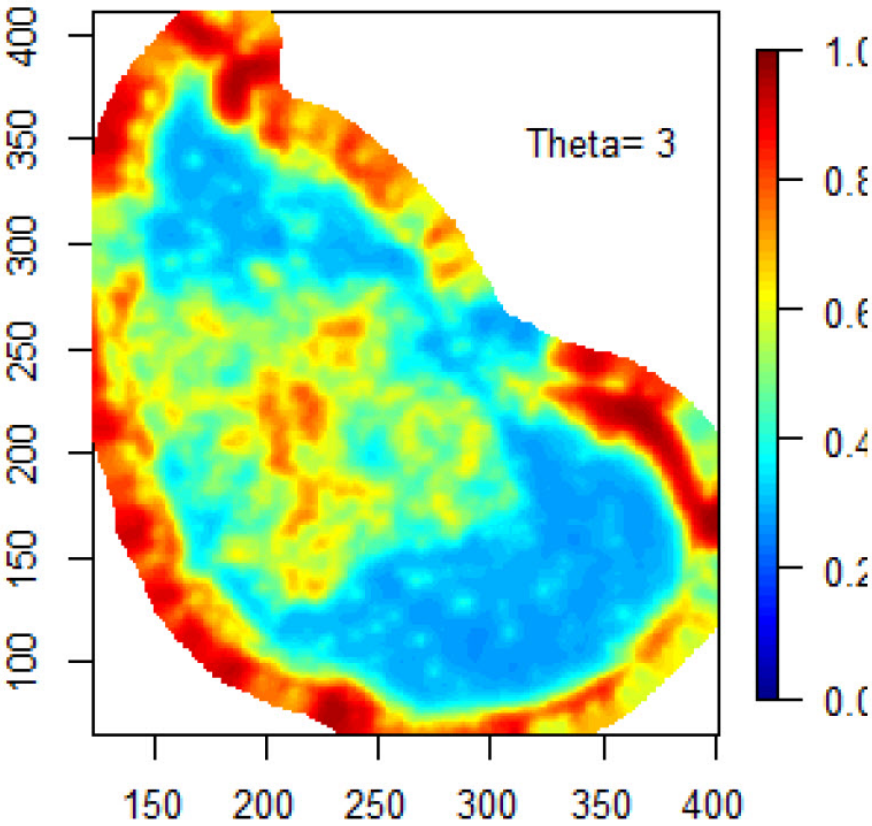

Slice of Posterior probability map

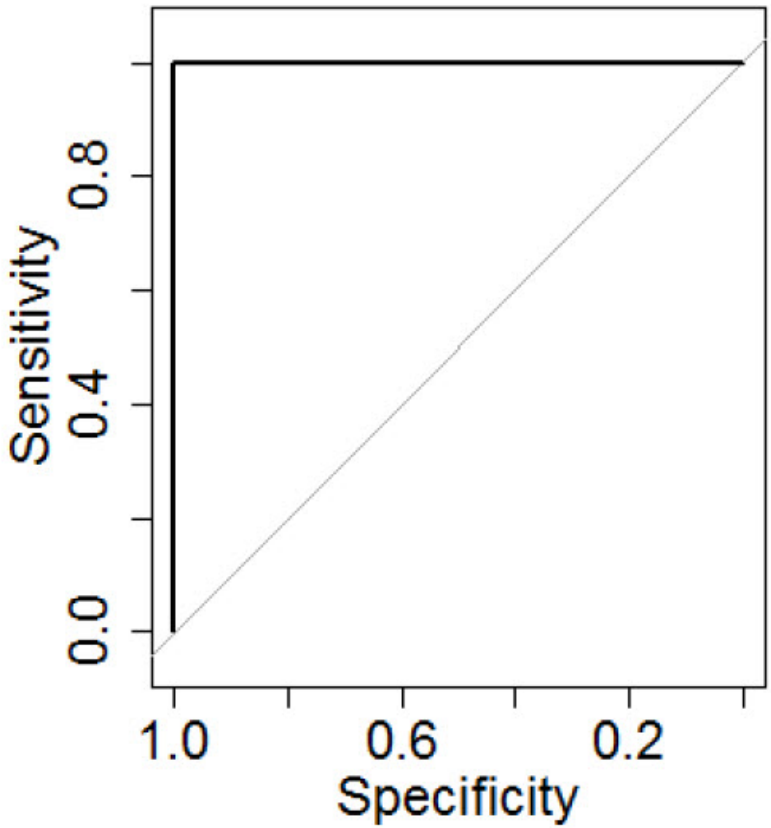

ROC curve using posterior probability as the classifier

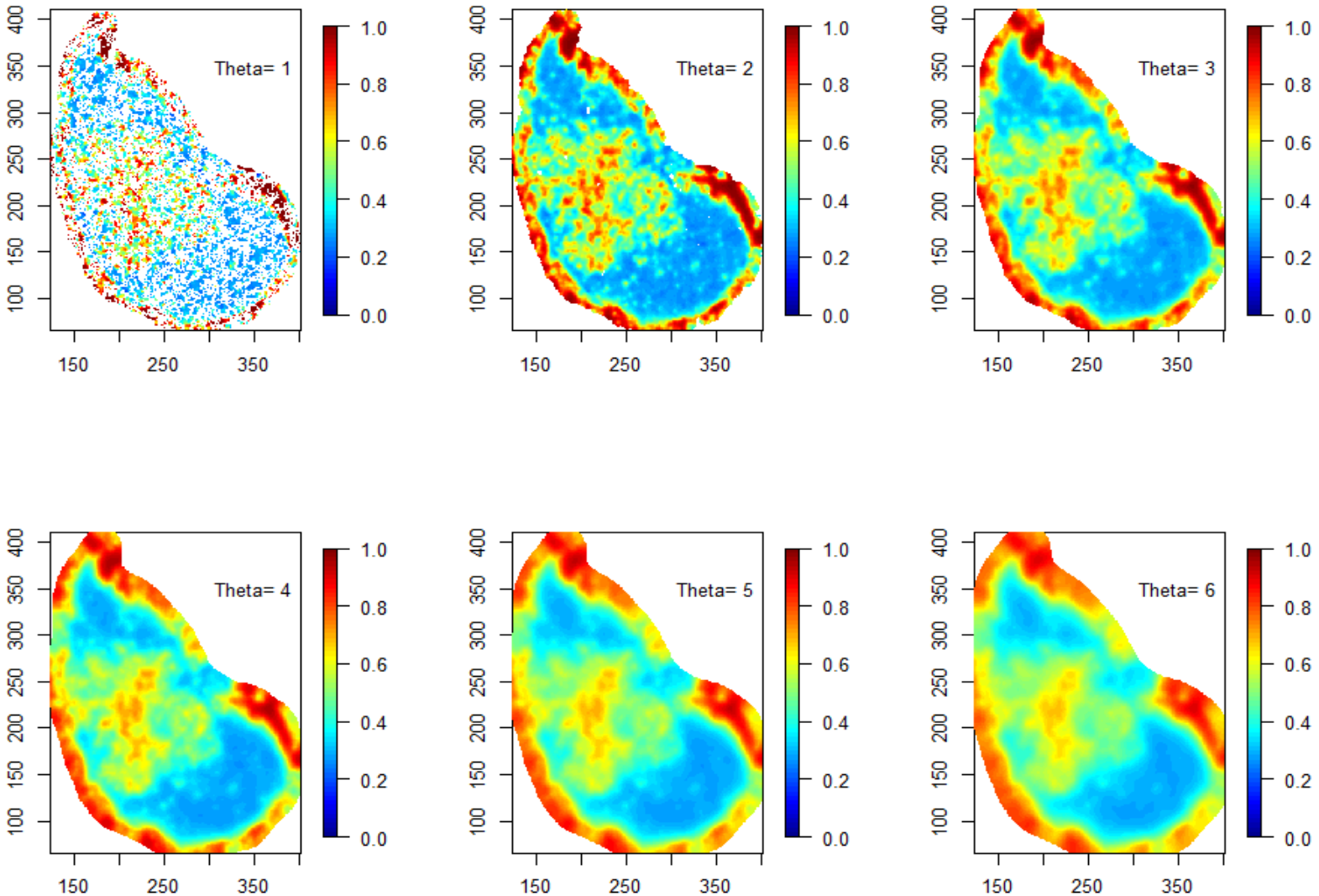

HC Pat 8 Slice 4 K=5 10,000 voxels

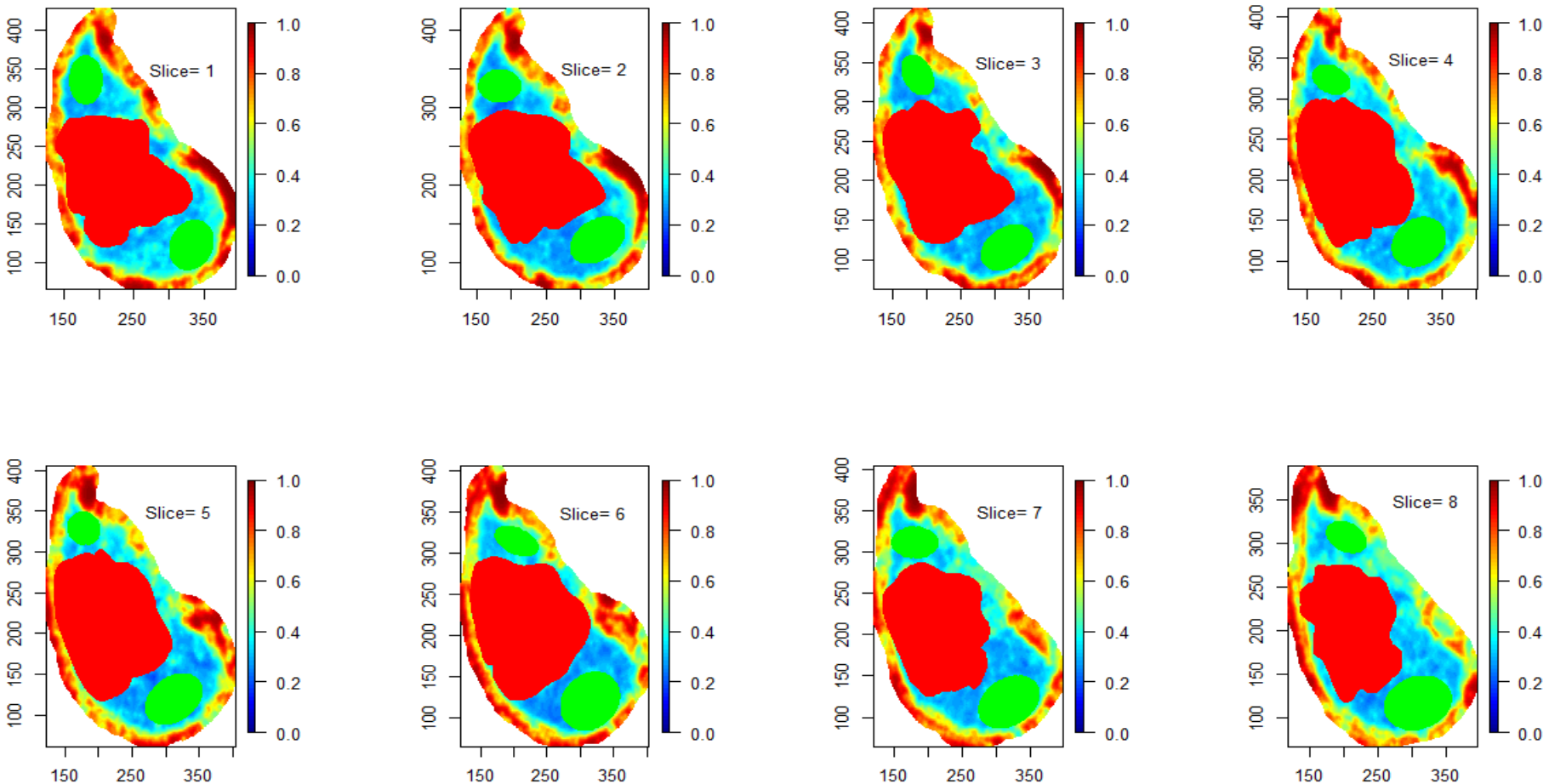

HC Pat 8 all slices K=5 theta = 3 10,000 voxels predicted based on the training set of slice 4

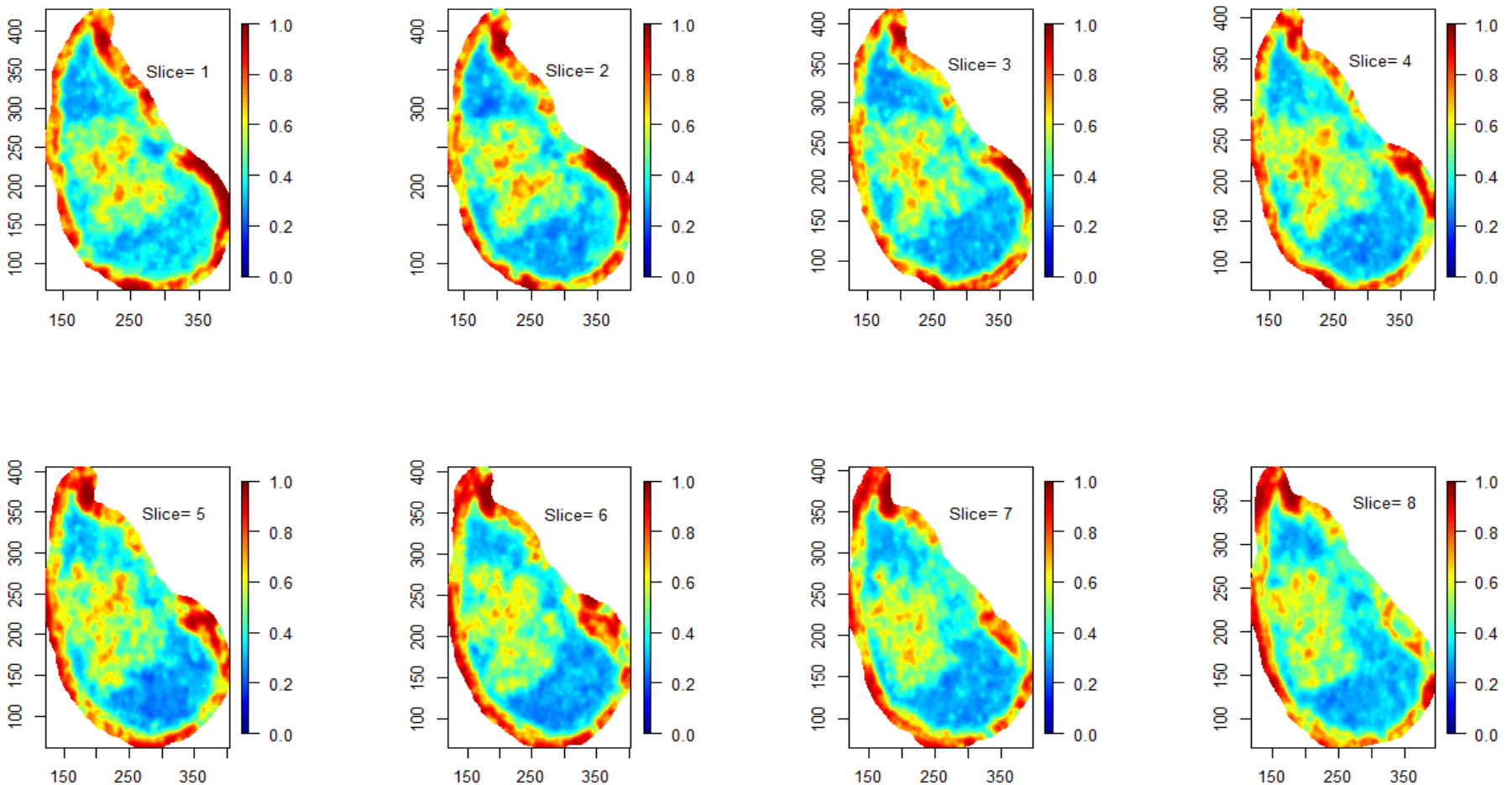

HC Pat 8 all slices K=5 theta = 3 10,000 voxels predicted based on the training set of slice 4

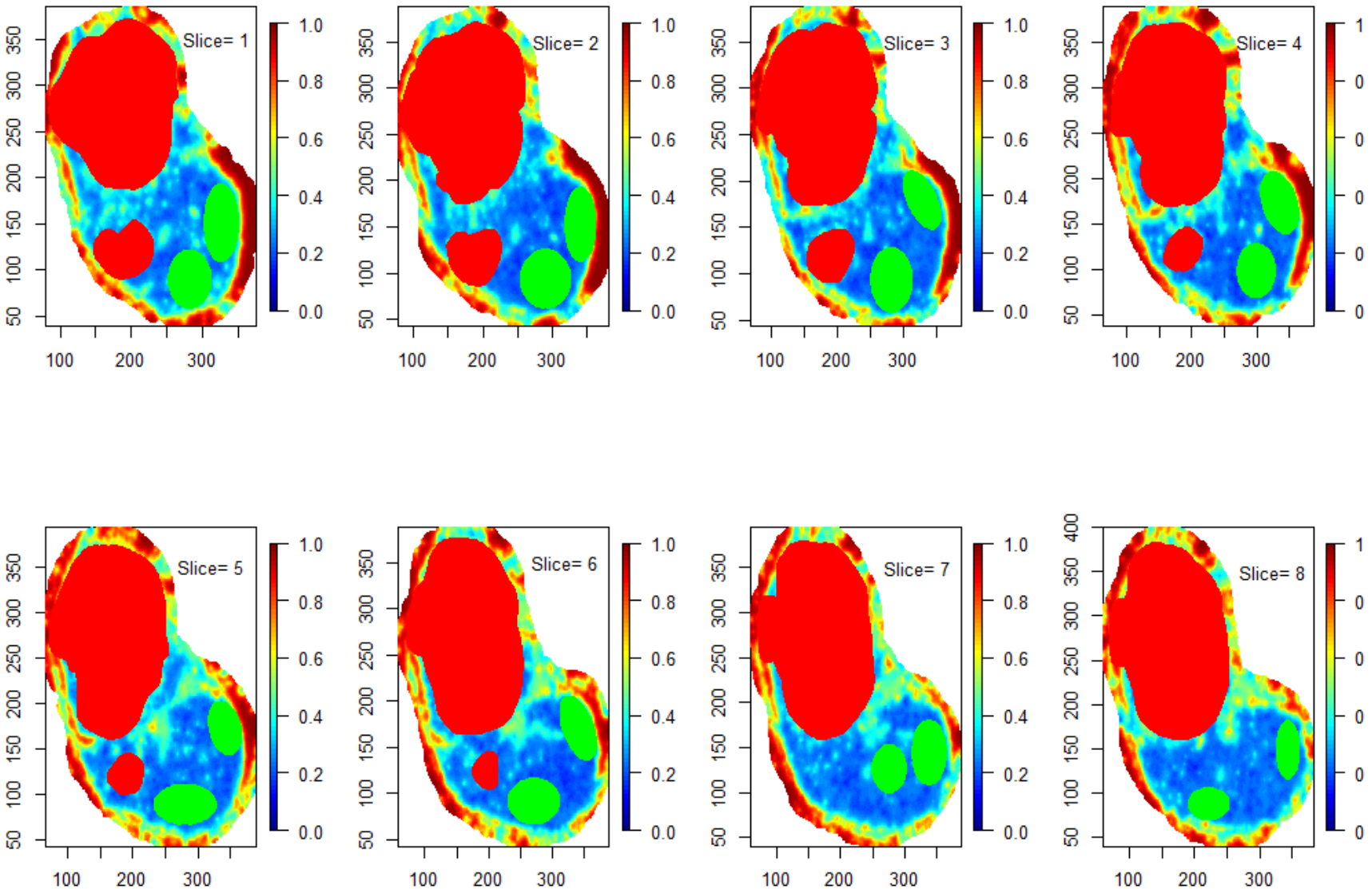
Slice= 1
Slice= 2
Slice= 3
Slice= 4
Slice= 5
Slice= 6
Slice= 7
Slice= 8

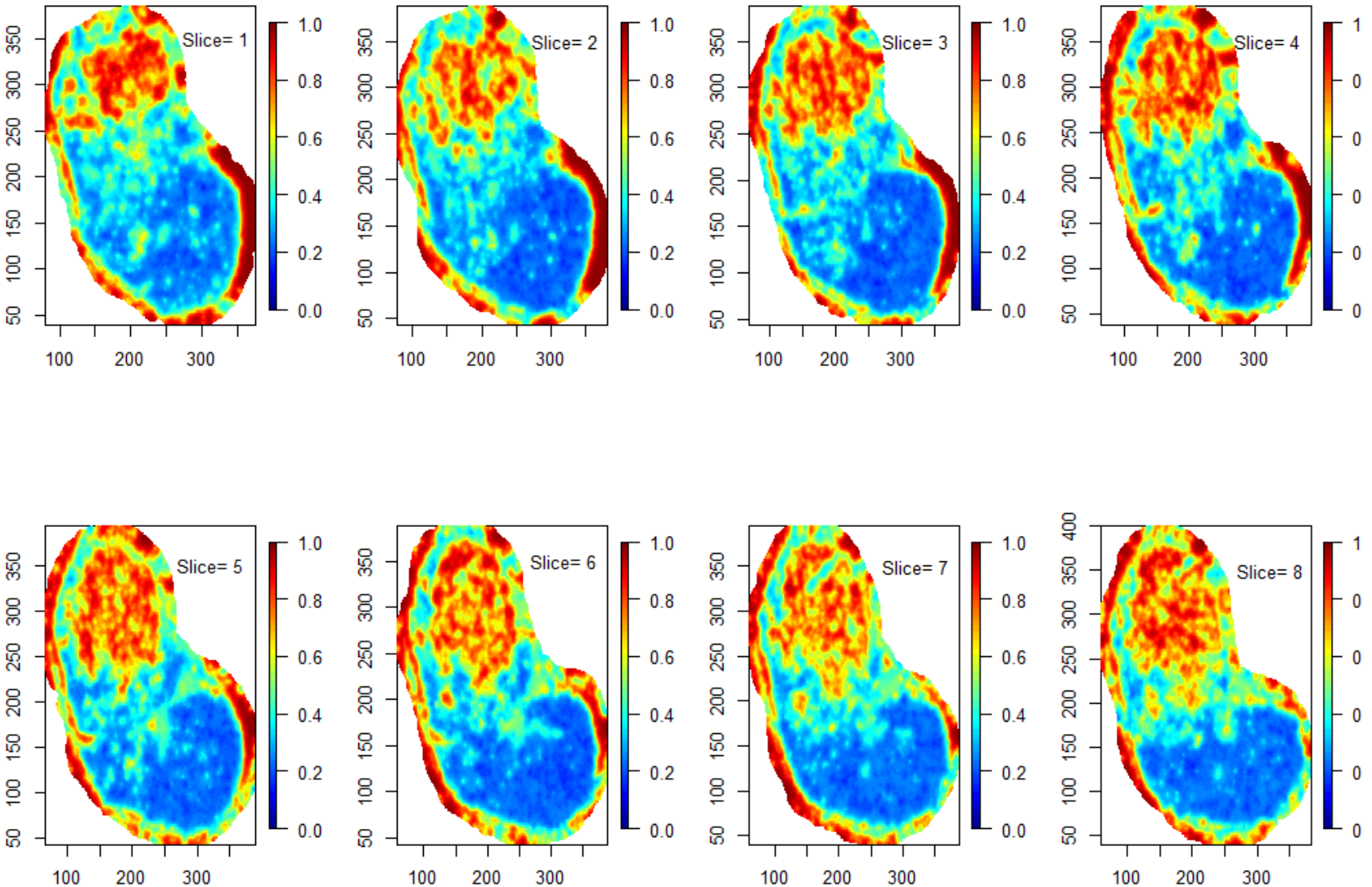
Slice= 1
Slice= 2
Slice= 3
Slice= 4
Slice= 5
Slice= 6
Slice= 7
Slice= 8

Functional Data Analysis of spatial-temporally correlated CTp curves

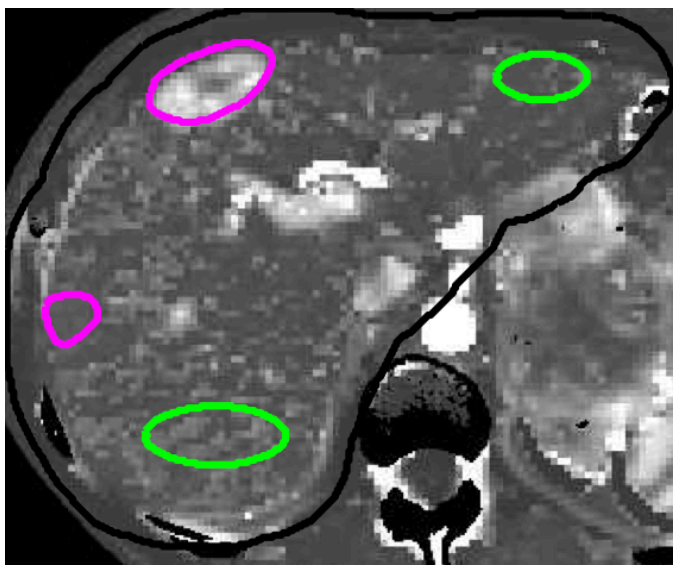

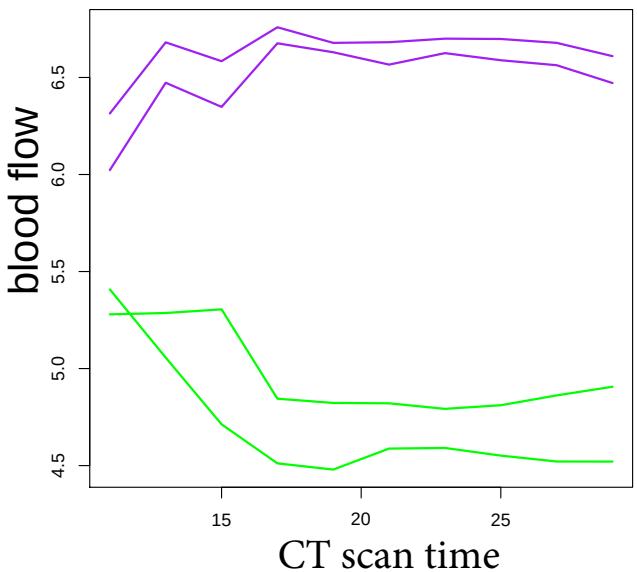

Summary

- Bayesian modeling is powerful tool for complex integration analysis
  - accounting for multiple source of variability
  - facilitates probabilistic inference
- General method offers the potential to improve classification performance in settings wherein multiple classification targets are evaluated within each subject
- Implications for any biomedical application that utilizes biomarkers to identify features intrinsic to a particular disease at multiple interdependent sites within an organ

Papers

1. B. P. Hobbs and C. S. Ng, (2015). "Inferring stable acquisition durations for applications of perfusion imaging in oncology," *Cancer Informatics*
2. Y. Wang, B. P. Hobbs, J. Hu, C. S. Ng, and K. A. Do, (2015). "Predictive Classification of Correlated Targets with Application to Detection of Metastatic Cancer using Functional CT Imaging," *Biometrics*
3. B. P. Hobbs, P. F. Thall, and S. H. Lin (2015), "Bayesian Group Sequential Clinical Trial Design using Total Toxicity Burden and Progression-Free Survival," *Journal of the Royal Statistical Society Series C*
4. Y. Wang, J. Hu, K. A. Do, and B. P. Hobbs, "An Efficient Nonparametric Estimate for Spatially Correlated Functional Data," *submitted*